Oxygen Isotope anomalies of meteorites

H. Yurimoto (Hokudai)

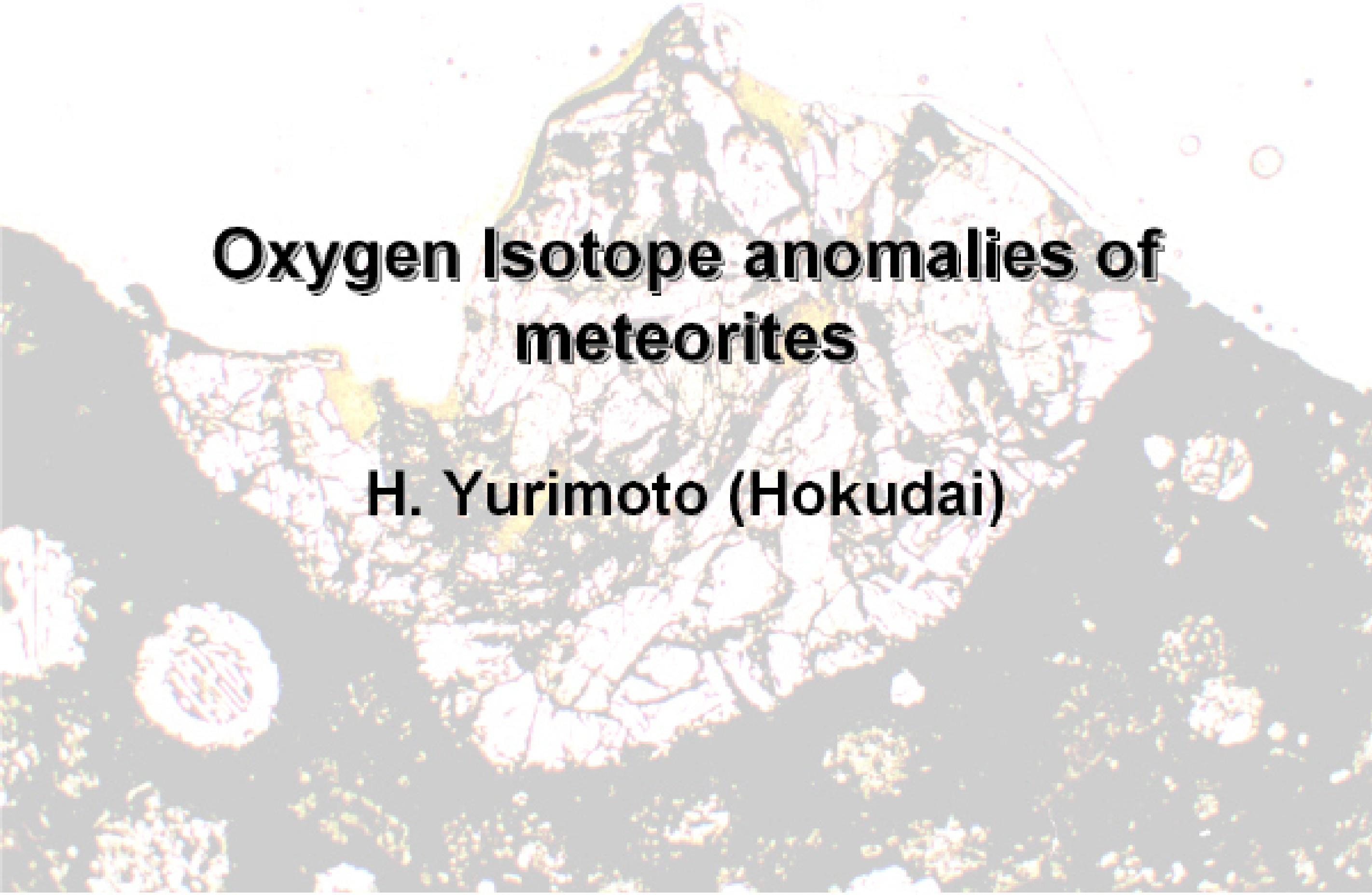

Oxygen

- The 3rd most abundant element in the solar system
- The most abundant element of the solid phases
- Best tracer for understanding the co-evolution of gas and solid components in the solar system

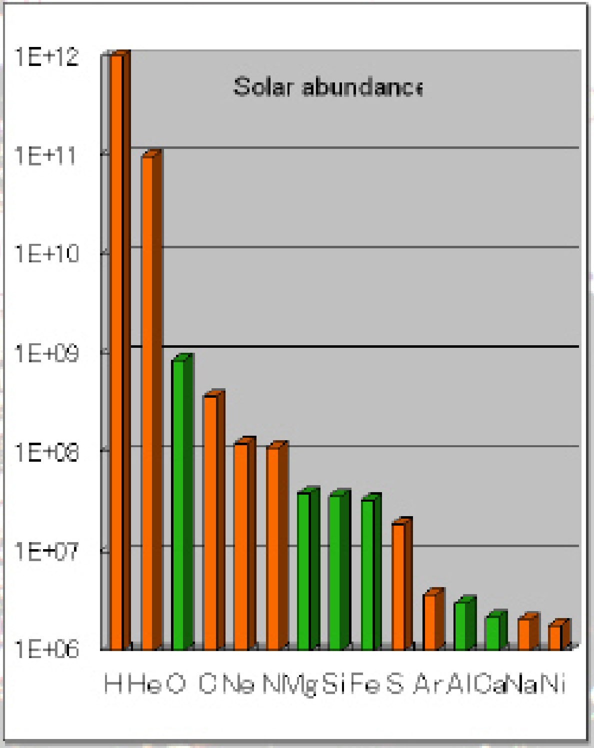

Oxygen isotopes

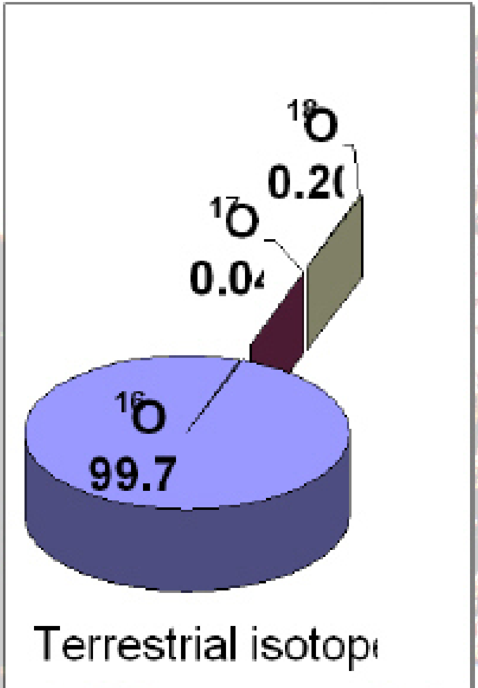

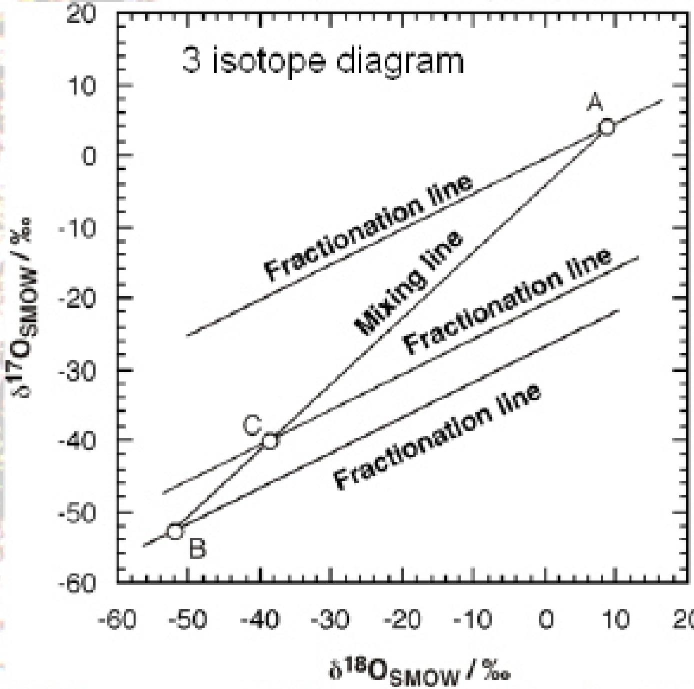

$$\delta^{i}O_{SMOW}\ (‰) = \{(^{i}O/^{16}O)_{Sample}/(^{i}O/^{16}O)_{SMOW} - 1\} \times 1000,\ \ i = 17\ or\ 18$$

O isotopic heterogeneity in the solar system

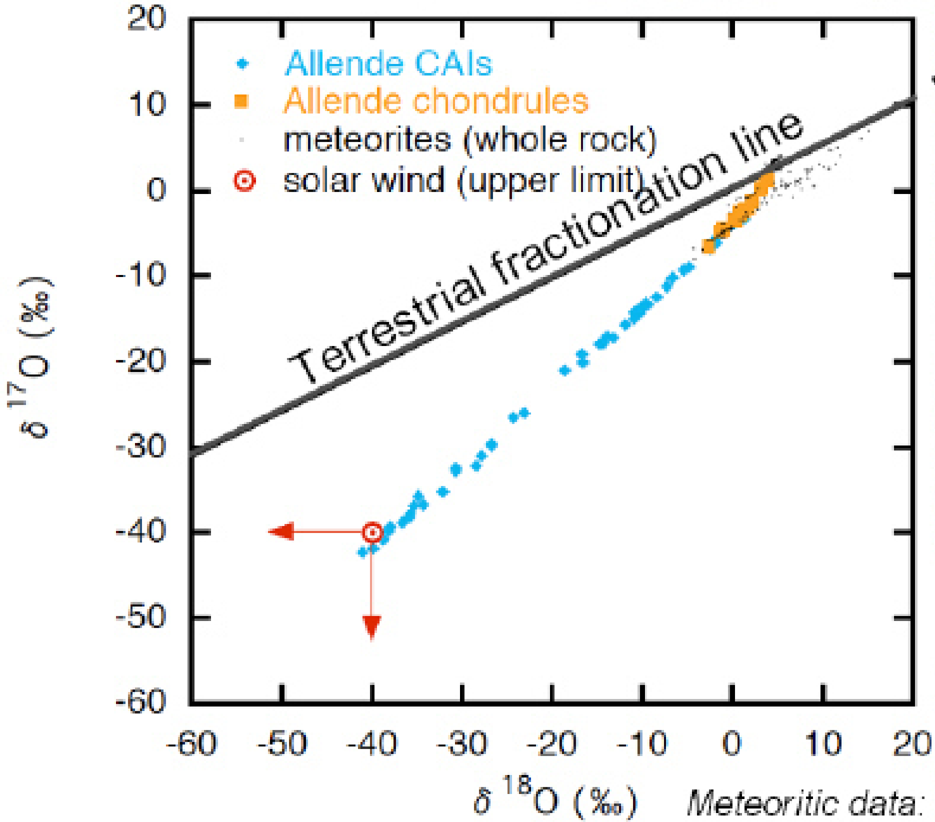

Components in Primitive Meteorites

- Meteorites: Building blocks of planets
- Mass-independent heterogeneity in O isotopic composition
- Only in oxygen isotopes
- Isotopes for other elements: Homogeneous, no anomaly

Meteoritic data: Clayton (1993) and others

O isotopic heterogeneity in the solar system

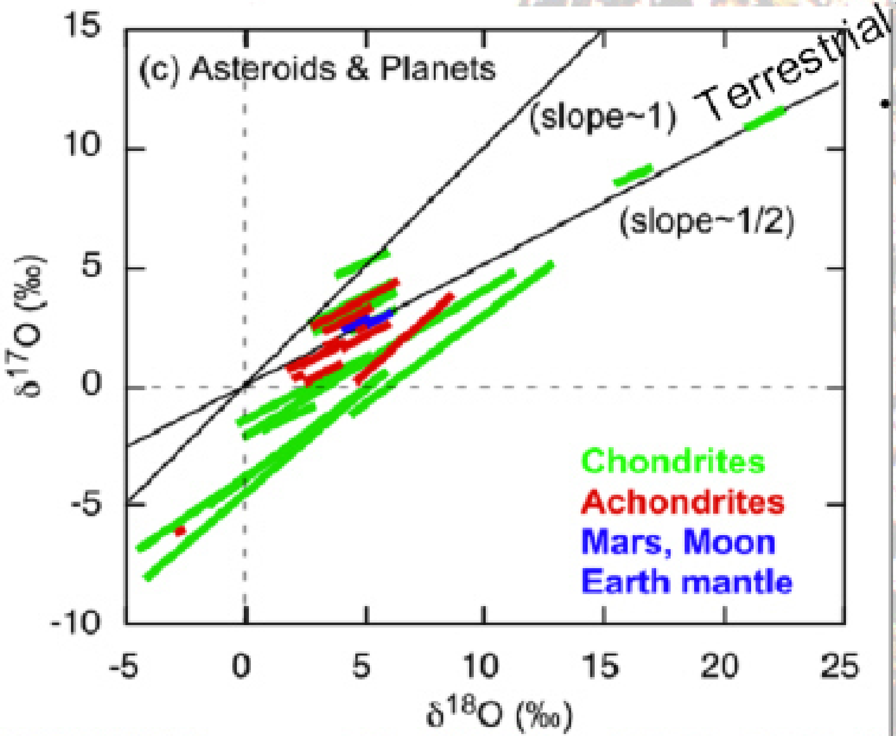

- Planets and asteroids
  - Mass-independent heterogeneity in O isotopic composition
  - Common feature at least in the inner solar system

Data: Clayton (1993) and others

O isotopic heterogeneity in the solar system

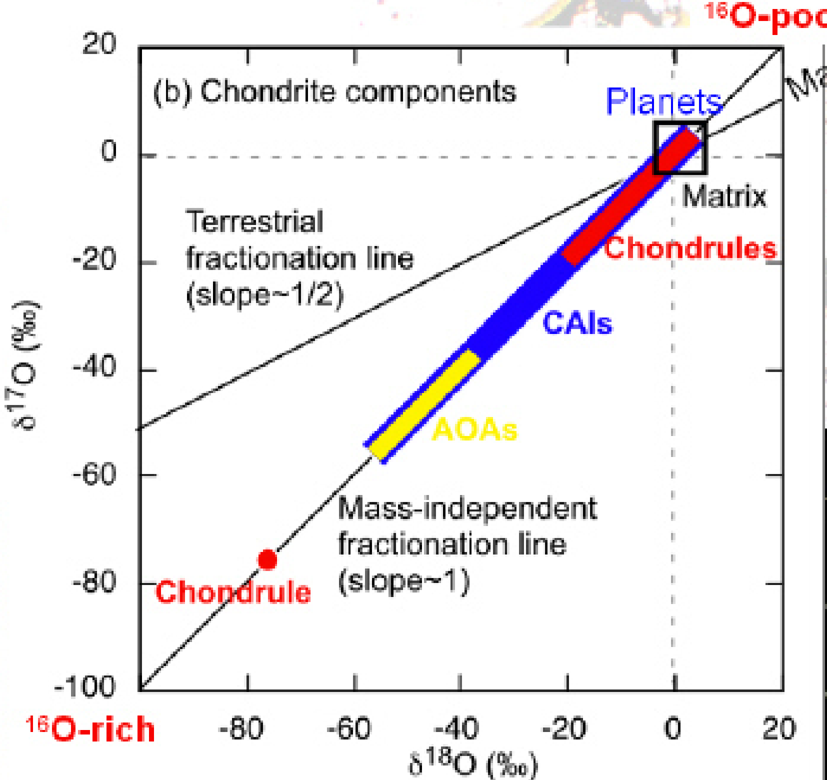

- **Mixing** between ^{16}O-rich and ^{16}O–poor end-member components
- Bulk O isotopic **composition of solar system**?

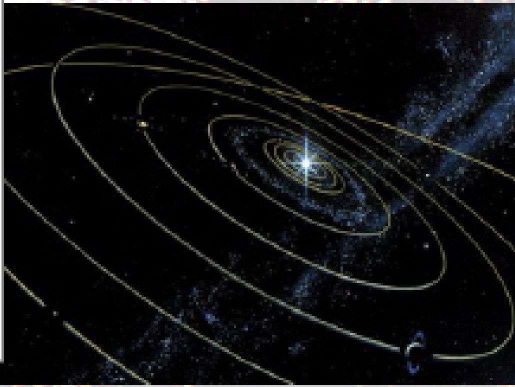

Data: Clayton (1993) and others

Refractory inclusions

- Oldest solids in the solar system
  - Pb-Pb: 4567 Ma (Amelin et al., 2002)
- Existence of live short-lived nuclides
  - ^{26}Al, ^{60}Fe, ^{10}Be, etc.
  - $(^{26}Al/^{27}Al)_0 \sim 6\times10^{-5}$ (Young et al., 200)
- Oxygen-isotope anomaly (Clayton et al., 1973)
- Providing essential information on the co-evolution of gas and solid components from the parent molecular cloud to the solar nebula
  - Review of O isotope distribution of refractory inclusions
  - Perspective of the nebular evolution

Refractory inclusions

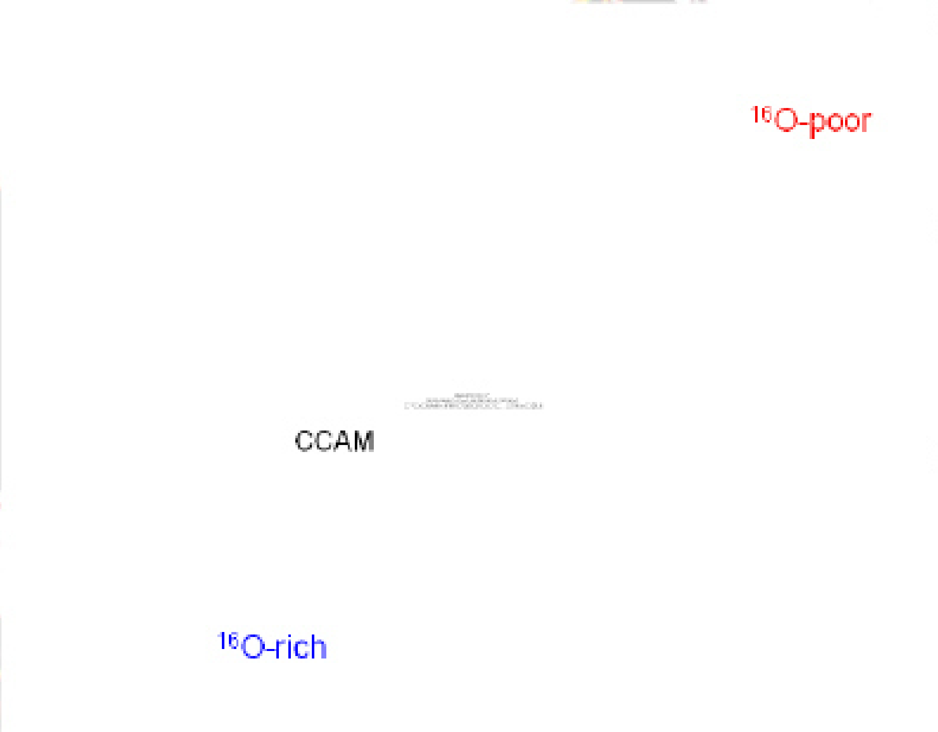

From Clayton (1993)

- Oldest solids in the solar system
  - Pb-Pb: 4567 Ma (Amelin et al., 2002)
- Oxygen-isotope anomaly (Clayton et al., 1973)
  - ^{16}O-rich
  - ^{16}O-poor
- Physical setting of the O isotopic reservoirs?

Refractory inclusions

- Fine-grained CAIs
  - Crystal size <50 µm
  - Ca-Al-rich minerals: e.g. melilite, spinel
- AOAs
  - Crystal size <50 µm
  - Mg-rich minerals: olivine
- Coarse-grained CAIs
  - Crystal size >50 µm
  - Ca-Al-rich minerals: e.g. melilite, spinel

No distinct boundary

Fine-grained CAIs

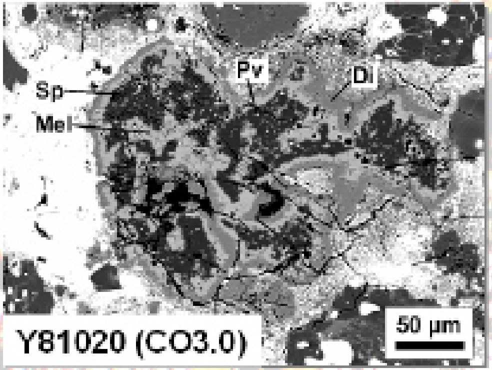

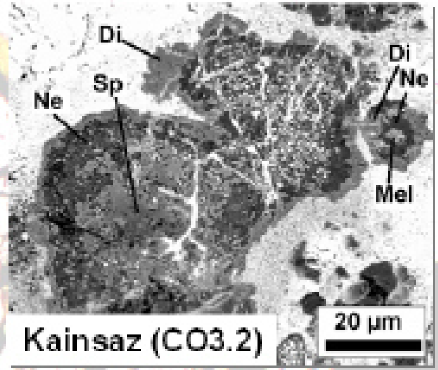

- Common in all chondrite groups
- Direct condensate from vapor
- Original structure and O-isotopic compositions: easily disturbed by aqueous alteration in the parent body (Wasson et al., 2001; Itoh et al., 2004)
- Need to select fresh primary phases

Fine-grained CAIs

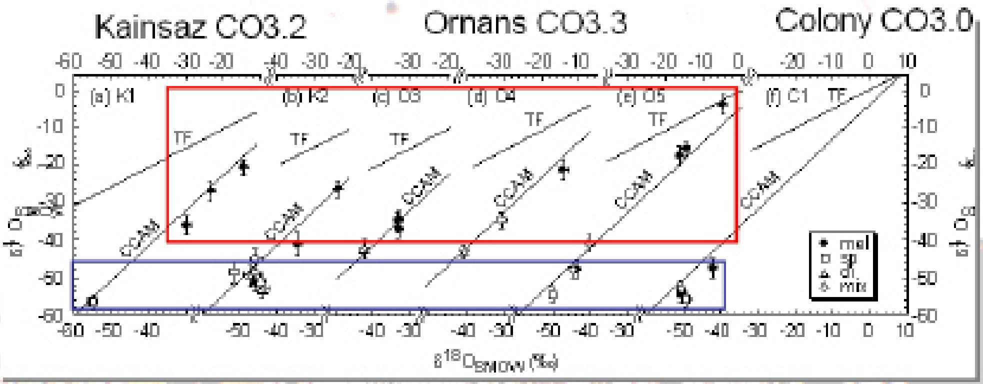

- Common in all chondrite groups
- Direct condensate from vapor
- Original structure and O-isotopic compositions: easily disturbed by aqueous alteration in the parent body (Wasson et al., 2001; Itoh et al., 2004)
- Need to select fresh primary phases
- Systematic measurements of O-isotopes
  - O, E, CV, CM, CO, CR, CB, CH chondrites

Fine-grained CAIs

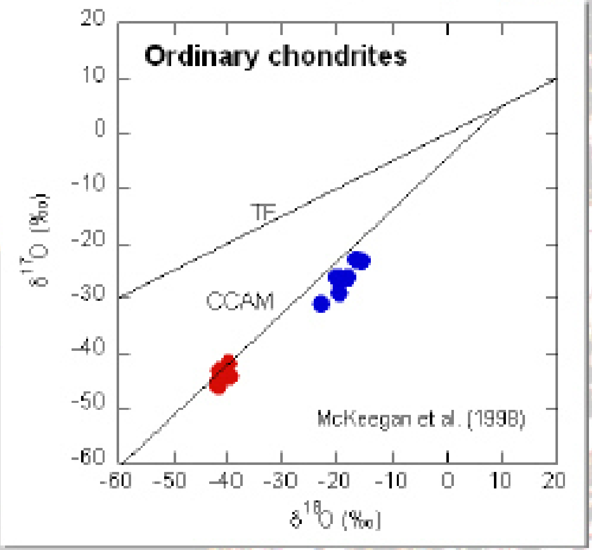

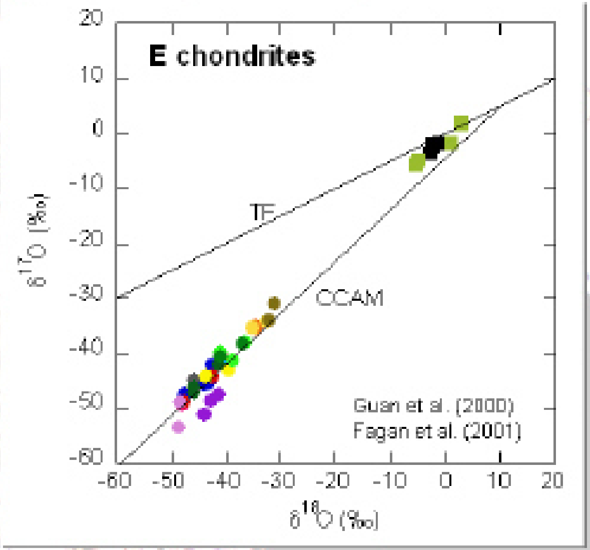

- Uniform composition among CAI minerals in a CAI
- Along to CCAM line
- ^{16}O-rich: majority, ^{16}O-poor: minority

Fine-grained CAIs

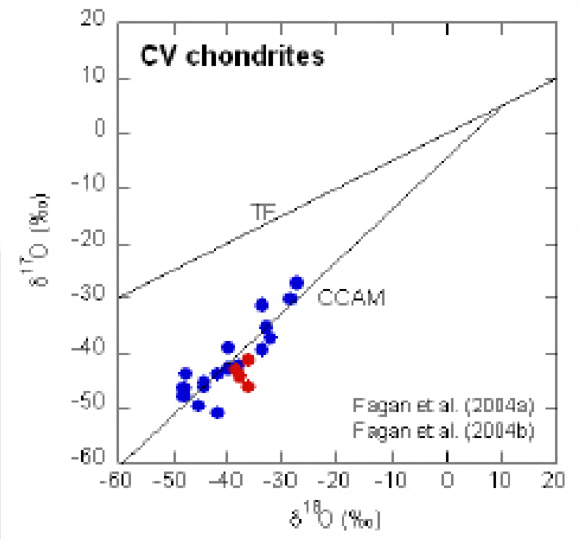

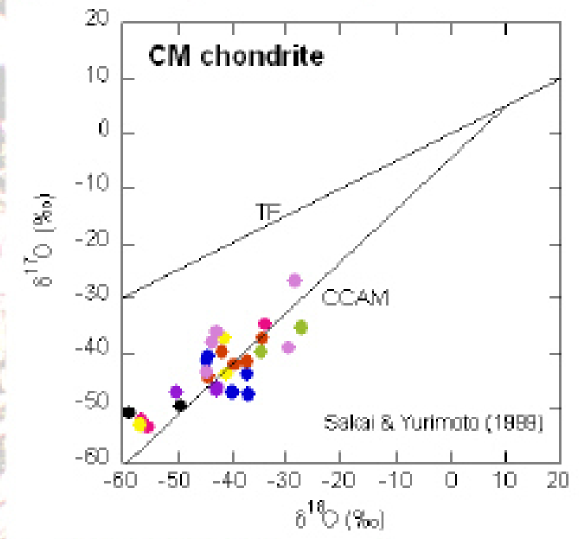

- Uniform composition among CAI minerals in a CAI
- Along to CCAM line
- ^{16}O-rich: majority, ^{16}O-poor: not found

Fine-grained CAIs

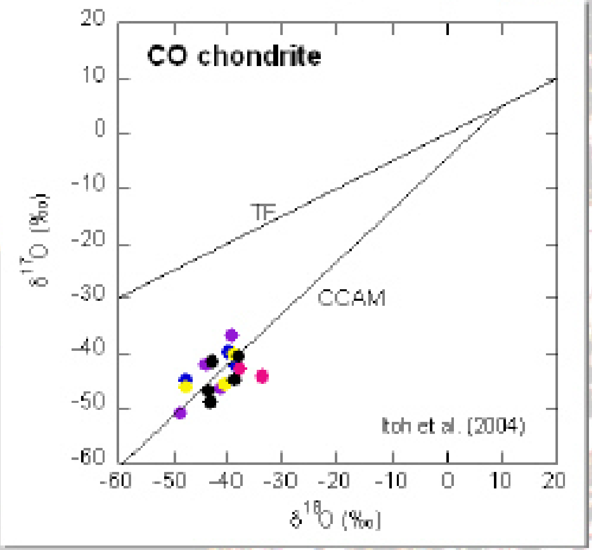

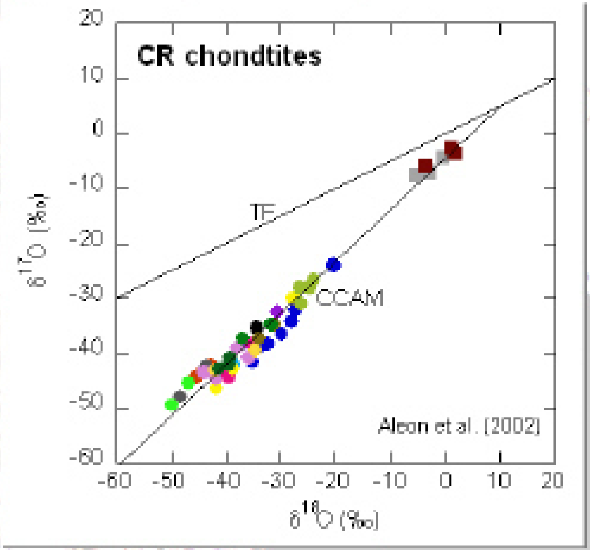

- Uniform composition among CAI minerals in a CAI
- Along to CCAM line
- ^{16}O-rich: majority, ^{16}O-poor: minority

Fine-grained CAIs

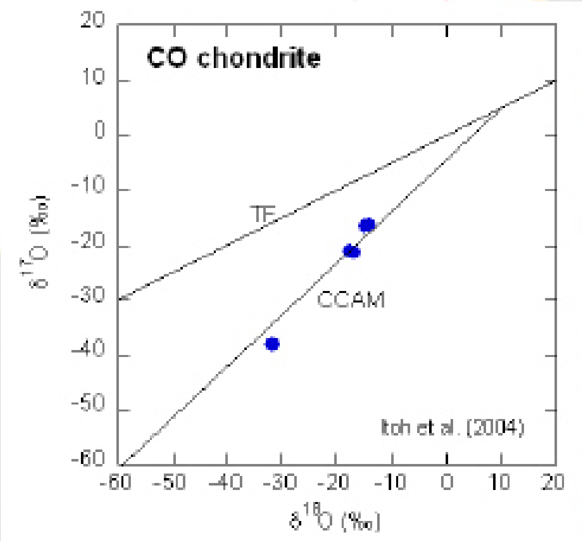

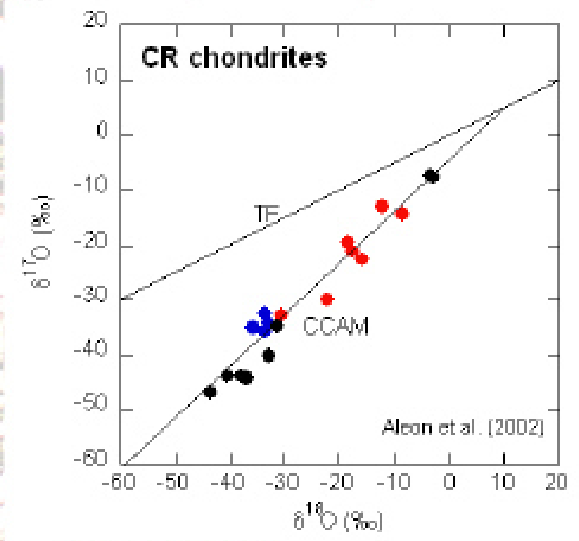

- Heterogeneous composition among CAI minerals in a CAI
- Along to CCAM line
- Incomplete melting texture

Fine-grained CAIs

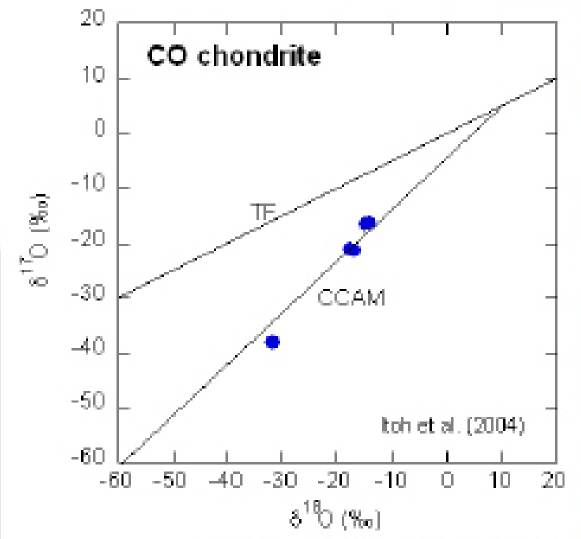

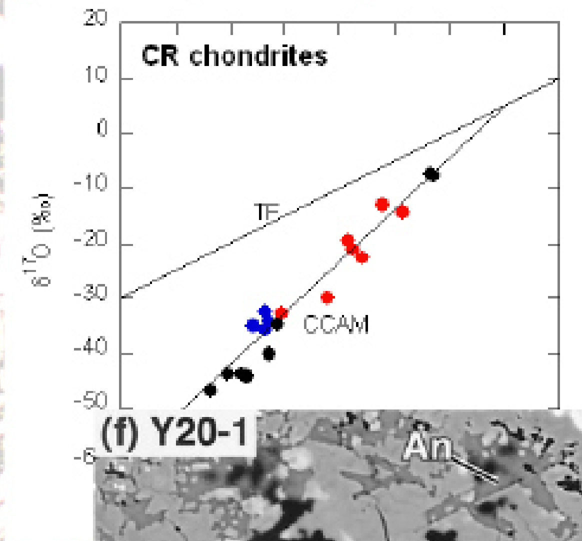

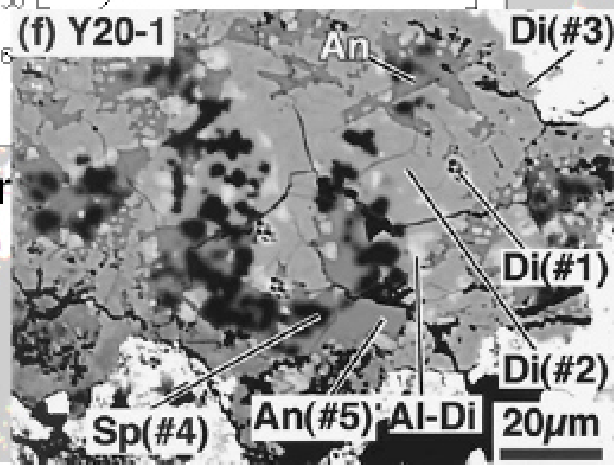

- Heterogeneous composition ar
  CAI
- Along to CCAM line
- Incomplete melting texture

Fine-grained CAIs

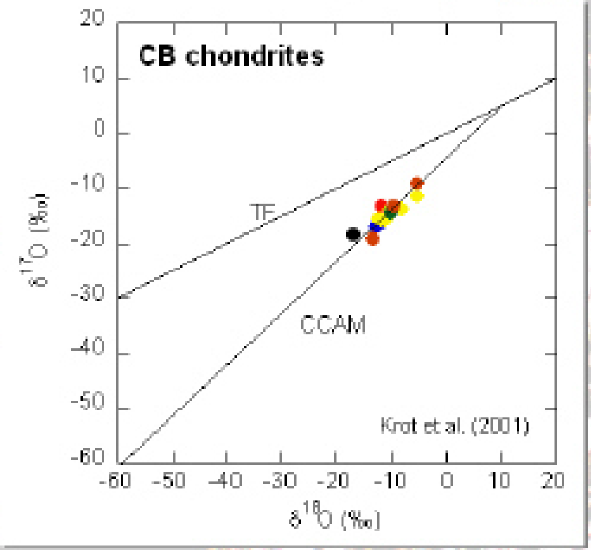

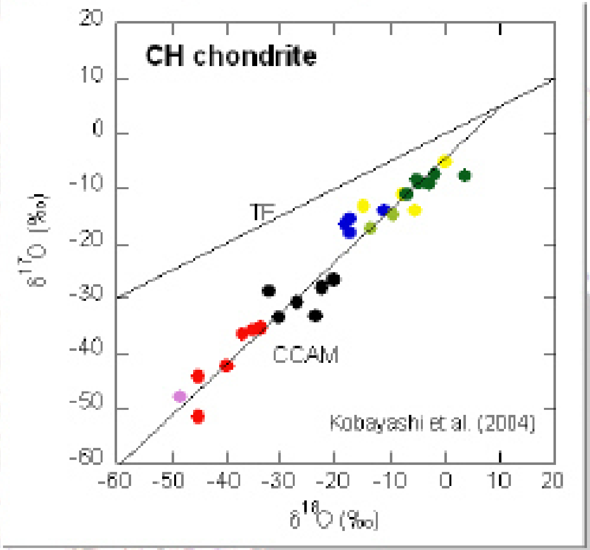

- Uniform composition among CAI minerals in a CAI
- Along to CCAM line
- ^{16}O-rich: not found, ^{16}O-poor: majority; for CB
- Ranges from ^{16}O-rich to ^{16}O-poor: for CH

Fine-grained CAIs (FGIs)

- Most FGIs have uniform O isotopic composition; indicating formation of each FGI completed in a single O isotopic reservoir.
- Most FGIs formed in an ^{16}O-rich gas.
- Some FGIs formed in an ^{16}O-poor gas.
- Some FGIs formed in an ^{16}O-rich gas and then reheated in an ^{16}O-poor gas
- O isotopic compositions of gas varied from ^{16}O-rich to ^{16}O-poor through FGIs formation period.
- FGIs formation period: ~2My?
  - $(^{26}Al/^{27}Al)_0$=0 - 5×10^{-5}

Amoeboid olivine aggregates (AOAs)

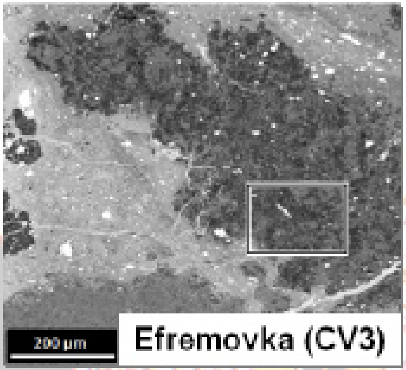

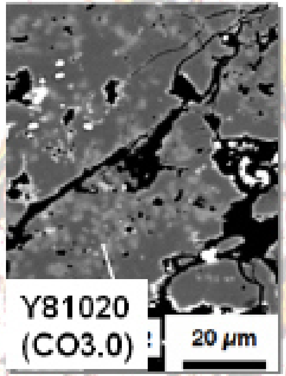

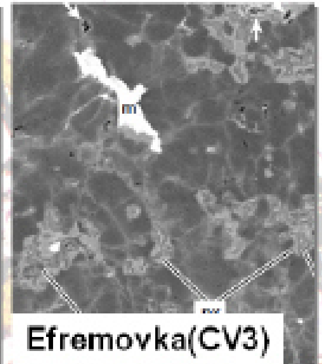

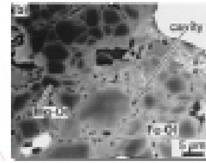

Allende
(CV3)

- Common in all chondrite groups
- Direct condensate from vapor
- Original structure and O-isotopic compositions: easily disturbed by aqueous alteration in the parent body (Imai and Yurimoto, 2003, Fagan et al., 2004)
- Need to select fresh primary phases

Amoeboid olivine aggregates (AOAs)

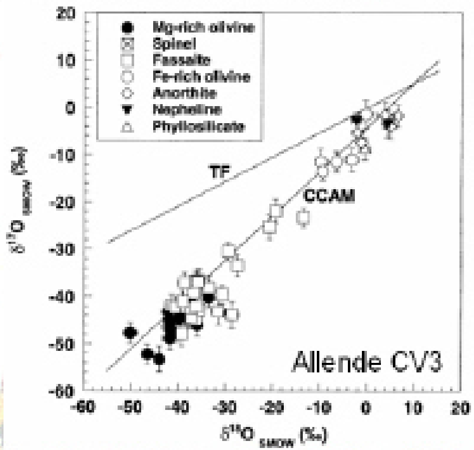

- Common in all chondrite groups
- Direct condensate from vapor
- Original structure and O-isotopic compositions: easily disturbed by aqueous alteration in the parent body (Imai and Yurimoto, 2003, Fagan et al., 2004)
- Need to select fresh primary phases

Amoeboid olivine aggregates (AOAs)

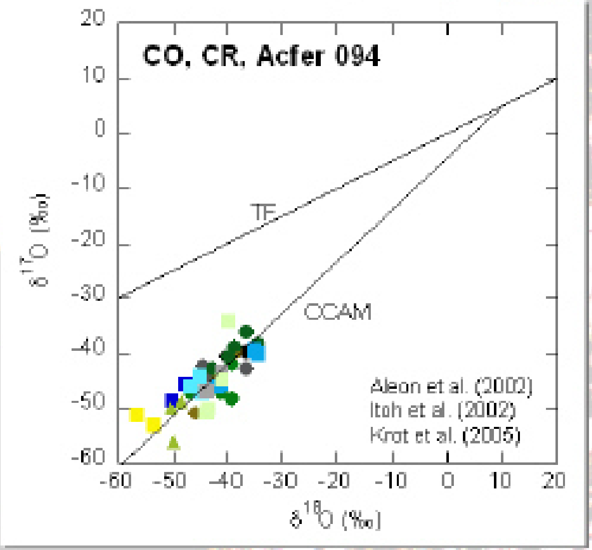

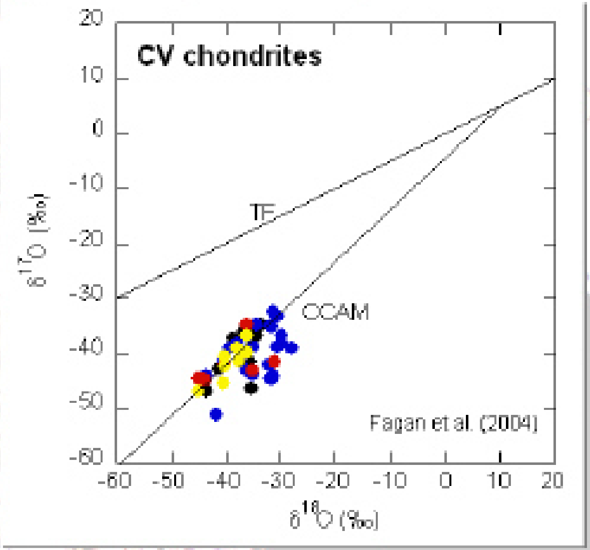

- Uniform composition among AOA minerals in an AOA
- Along to CCAM line
- ^{16}O-rich: majority, ^{16}O-poor: not found

Amoeboid olivine aggregates (AOAs)

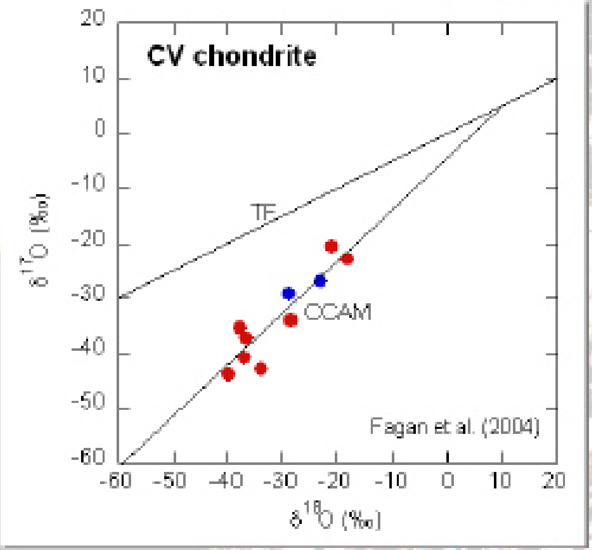

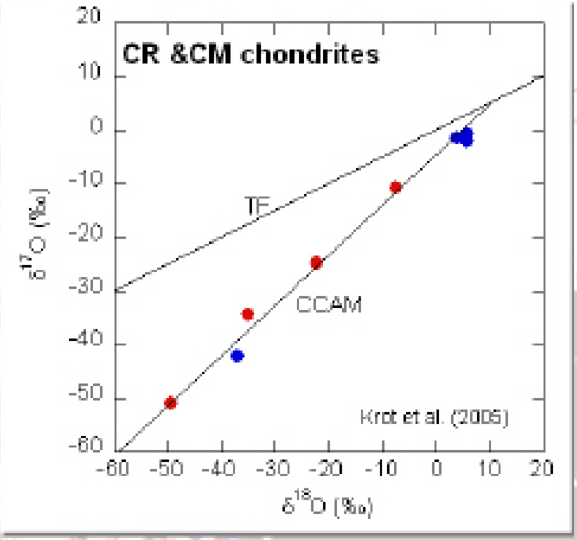

- Small enrichment of ^{16}O
- Heterogeneous composition among AOA minerals in a AOA
- Along to CCAM line
- Reaction or condensation texture

Amoeboid olivine aggregates (AOAs)

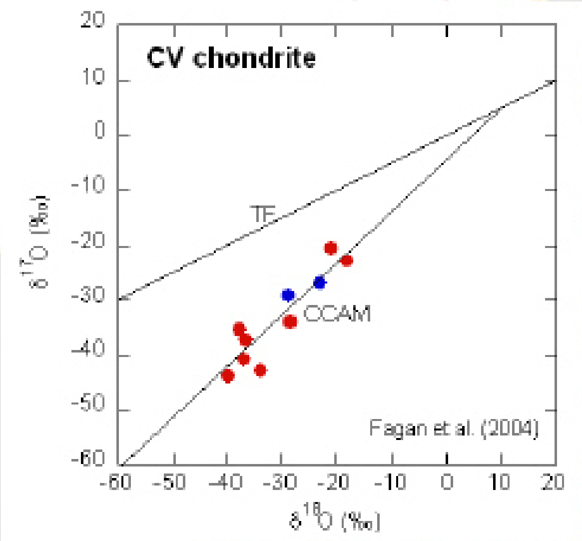

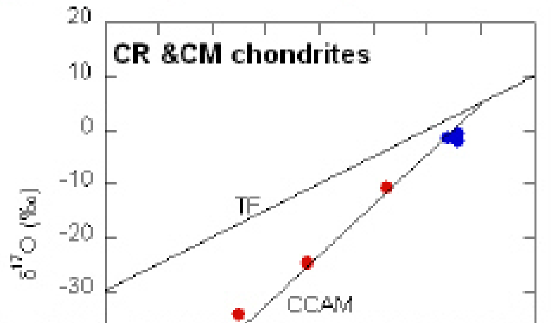

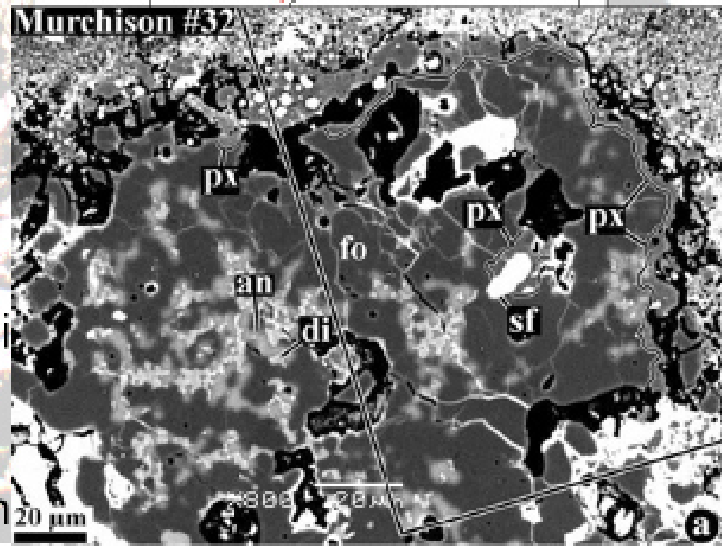

- Small enrichment of ^{16}O
- Heterogeneous compositi
a AOA
- Along to CCAM line
- Reaction or condensation

Amoeboid olivine aggregates (AOAs)

- Most AOAs have uniform O isotopic composition; indicating the formation of each AOA completed in a single O isotopic reservoir.
- Most AOAs formed in an ^{16}O-rich gas.
- Some AOA formed in an ^{16}O-rich gas and then reheated in an ^{16}O-poor gas
- O isotopic compositions of gas varied from ^{16}O-rich to ^{16}O-poor through AOAs formation period.
- AOAs formation period: ~2My??
  - $(^{26}Al/^{27}Al)_0$= ~3 x 10^{-5} (itoh et al. 2002)

Coarse-grained CAIs

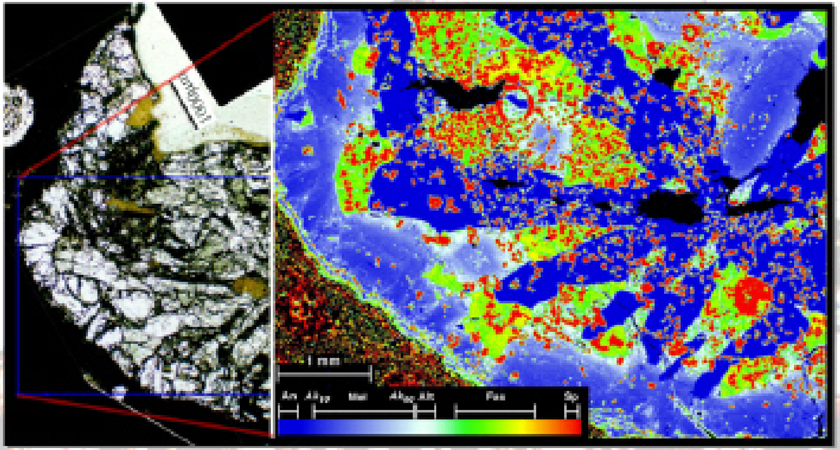

- Common in CV chondrites, but rare in other groups
- Crystallized from Ca-Al-rich liquid
- Because of the large crystal size, aqueous alteration is limited along grain boundaries and cracks.
- Complex thermal histories

Coarse-grained CAIs

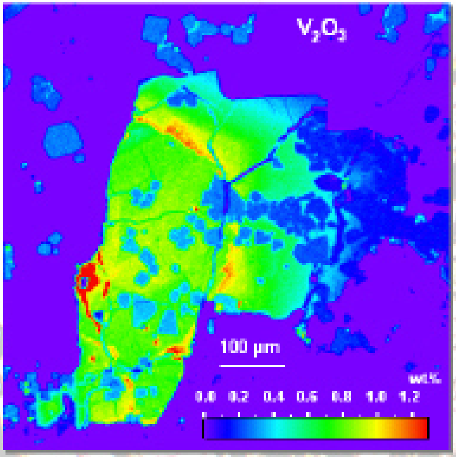

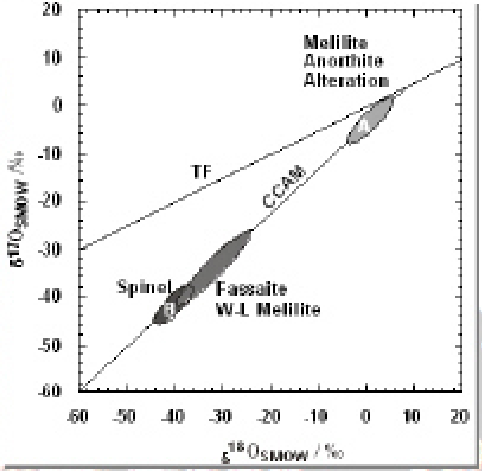

- Common in CV chondrites, but rare in other groups
- Crystallized from Ca-Al-rich liquid
- Because of the large crystal size, aqueous alteration is limited along grain boundaries and cracks.
- Complex thermal histories
- O isotope heterogeneity is common among crystals

Coarse-grained CAIs

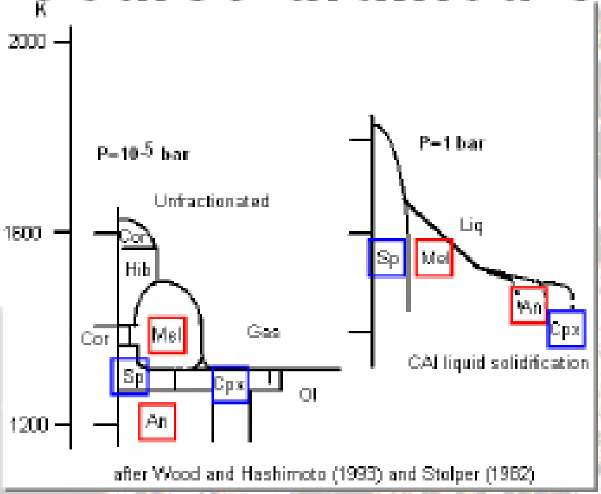

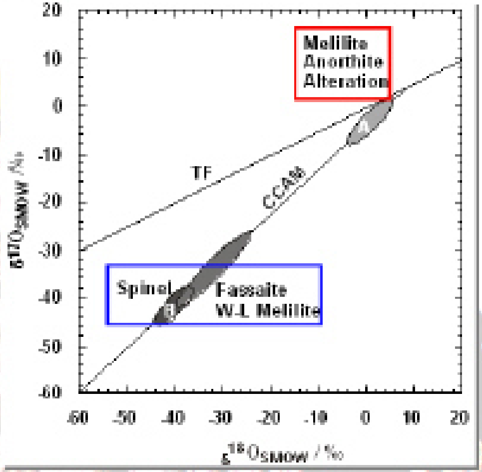

- Crystallized from Ca-Al-rich liquid
- Because of the large crystal size, aqueous alteration is limited along grain boundaries and cracks.
- Complex thermal histories
- O isotope heterogeneity is common among crystals
  - The heterogeneity is inconsistent with simple crystallization sequence from liquid or from gas

Coarse-grained CAIs (CGIs)

- CGI formation started in an ^{16}O-rich gas.
- All CGIs ever found were processed thermally in an ^{16}O-poor gas.
- O isotopic compositions of gas varied through CGIs formation period.

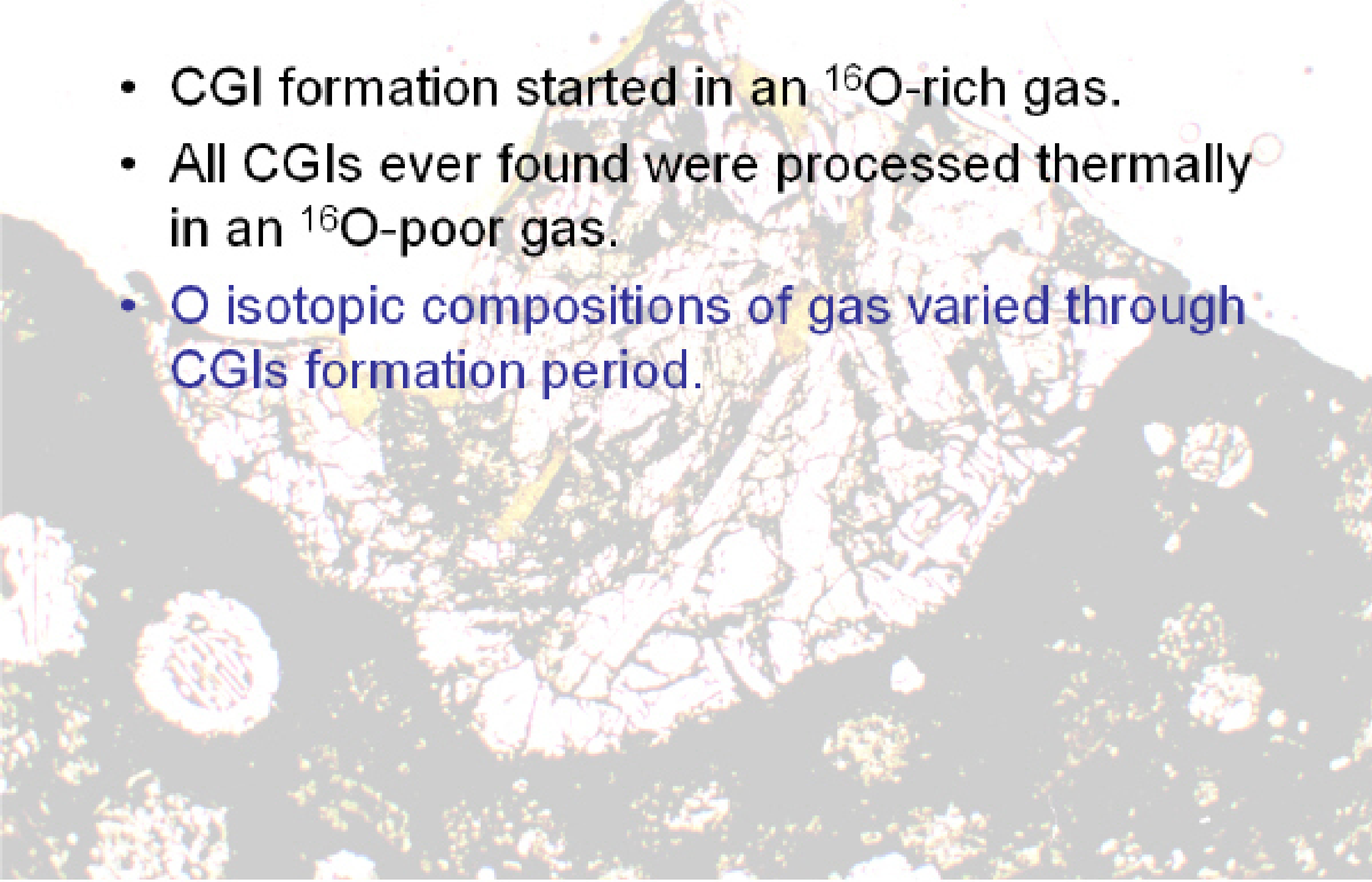

Implication to the nebula evolution

- The similar O-isotopic characteristics among FGIs, AOAs and CGIs indicate that refractory inclusions were co-genetic.
- O isotopic compositions of the solar nebula was originally ^{16}O-rich and shifted to ^{16}O-poor with time.
  - This is consistent to a global O isotopic evolving model of planetary disk (e.g. Yurimoto and Kuramoto, 2004).
- However, O isotopic compositions in the refractory inclusion forming region seems to be non-monotonically shifted from ^{16}O-rich to ^{16}O-poor.
- The non-monotonic O-isotope shifts may reflect local disk dynamics of refractory-inclusions forming region and conceal the global O isotope evolution of the disk under a cover.

Evidence 1: Overgrowth of ^{16}O-poor melilite

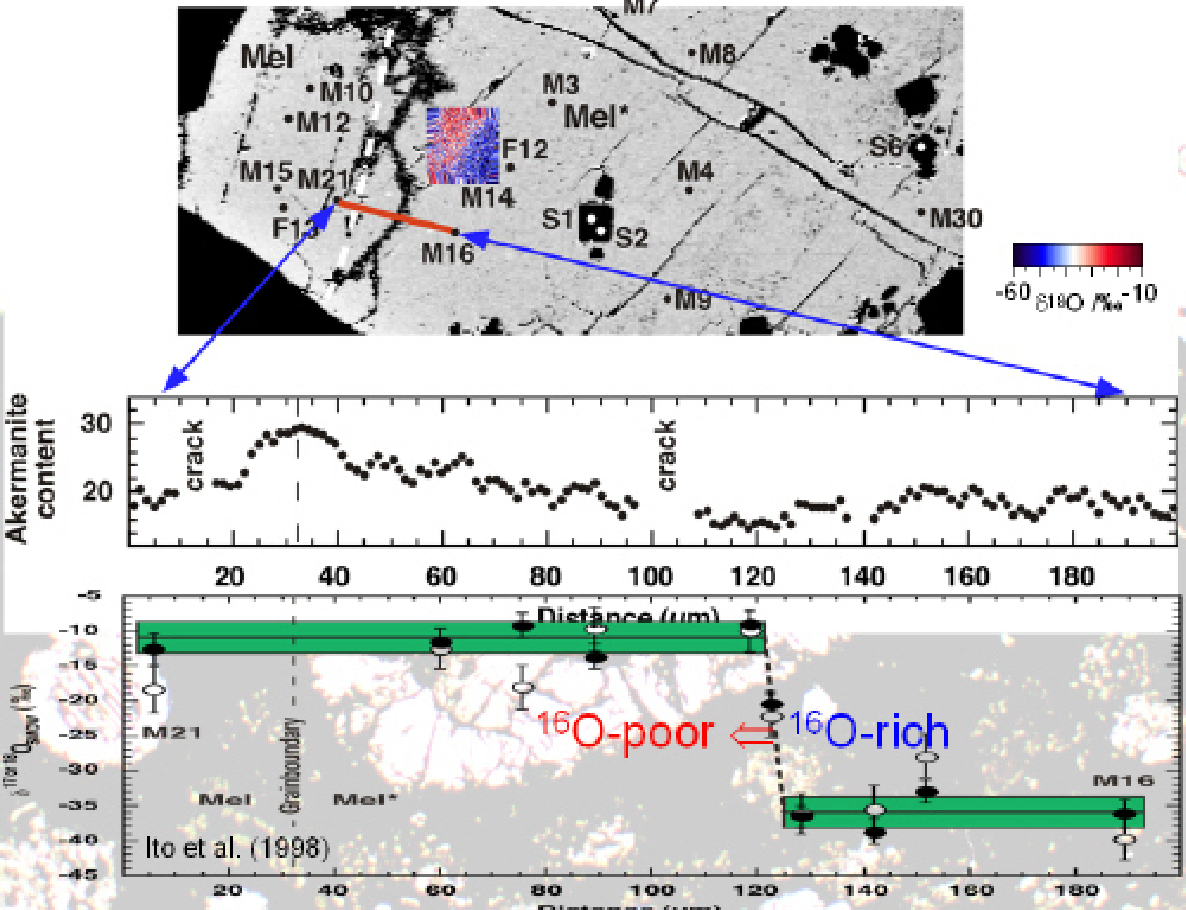

Evidence 1: Overgrowth of ^{16}O-poor melilite

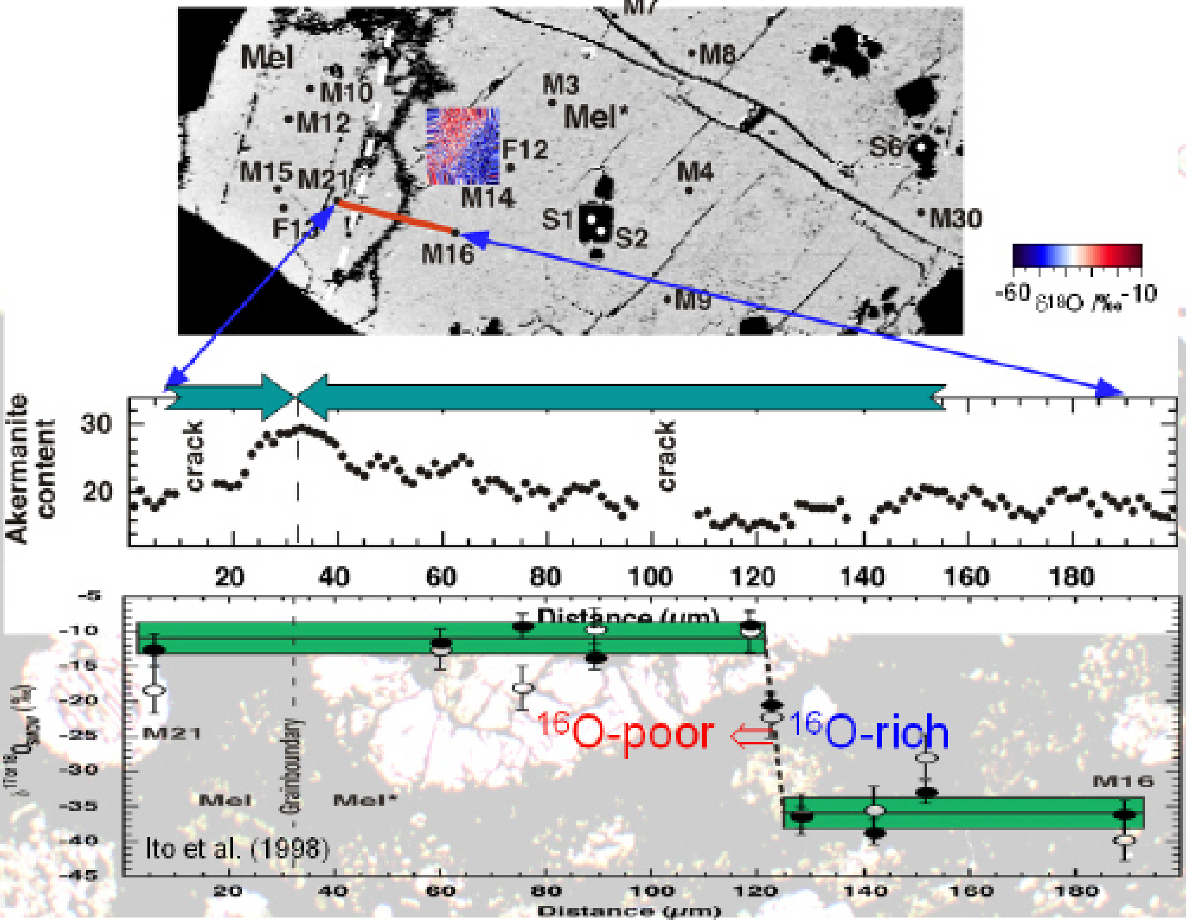

Evidence 1: Overgrowth of ^{16}O-poor melilite

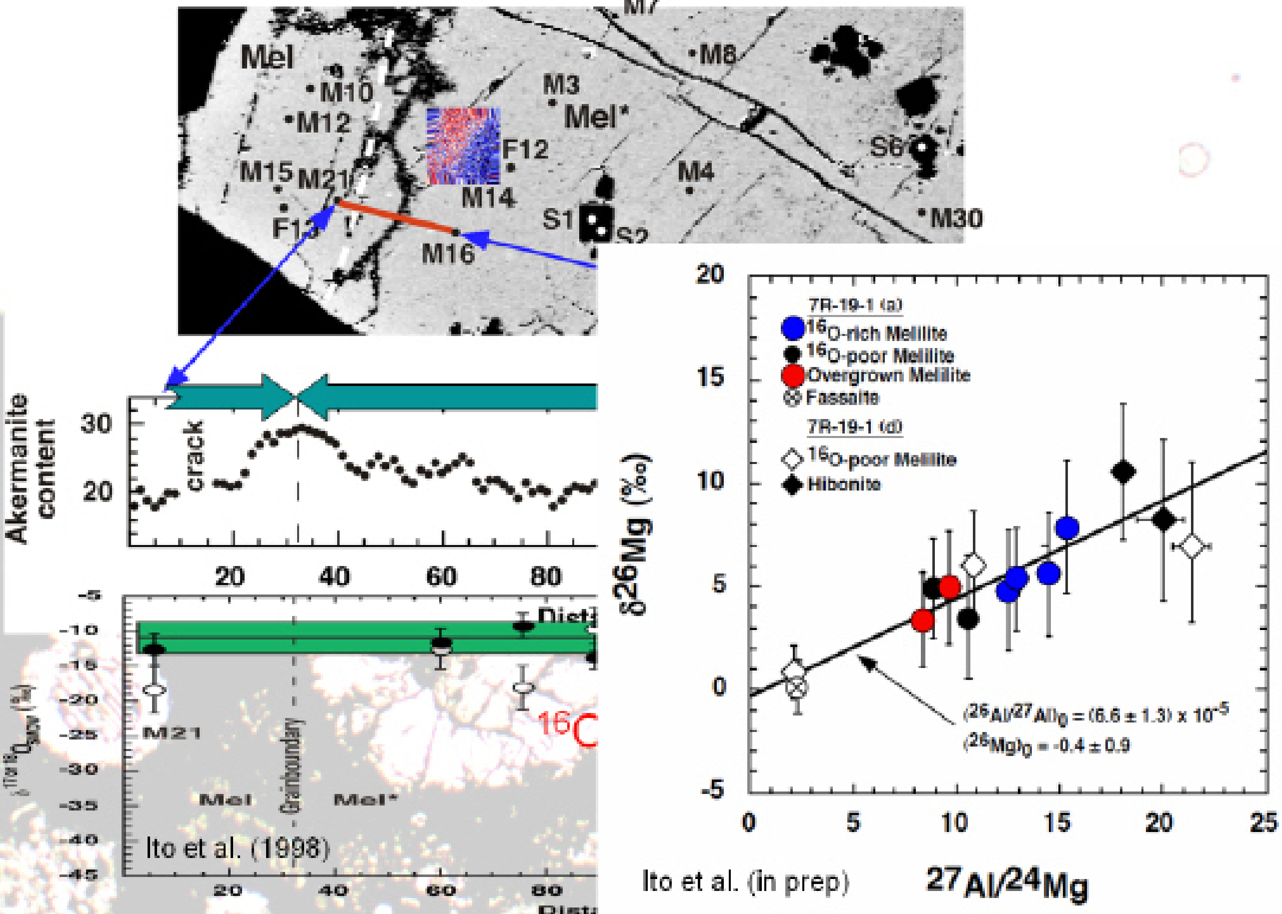

Evidence 2: Work-Lovering rim

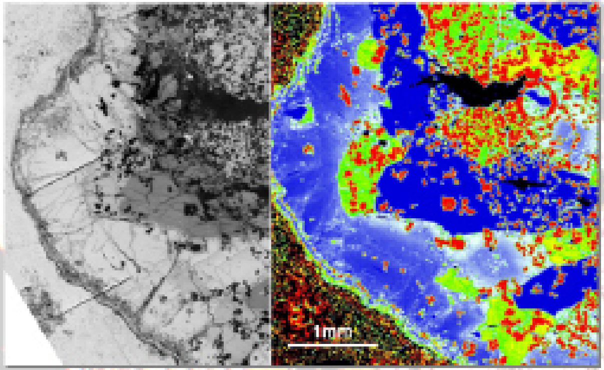

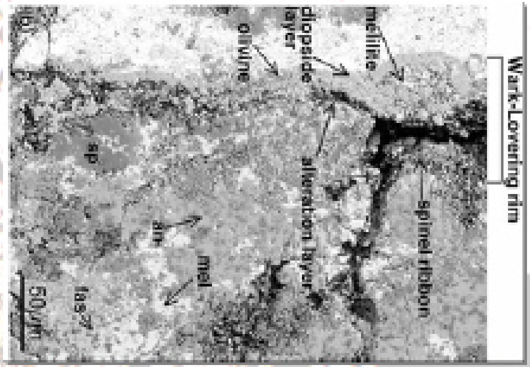

- Work-Lovering rim and accretionally olivine layer were condensed in ^{16}O-rich nebular gas (Krot et al., 2002).
- ^{16}O-poor minerals are observed inside CGIs, indicating ^{16}O-poor nebular gas.
- O isotopic shift: ^{16}O-rich → ^{16}O-poor → ^{16}O-rich

Evidence 3: A chondrule-bearing CAI, A5

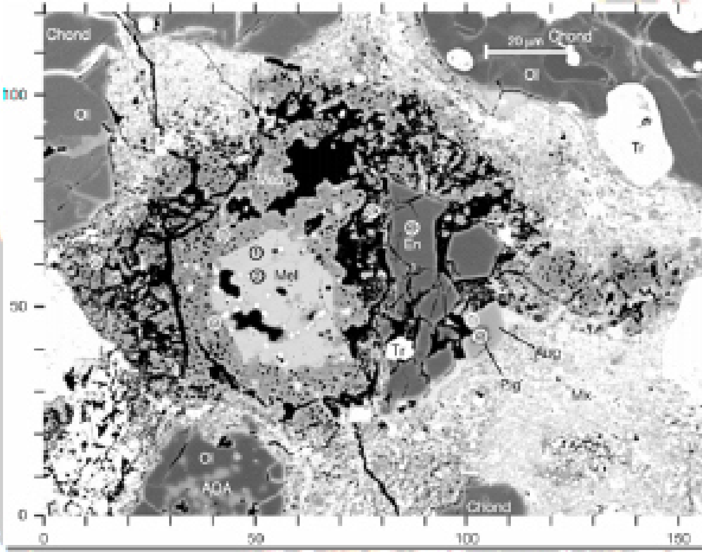

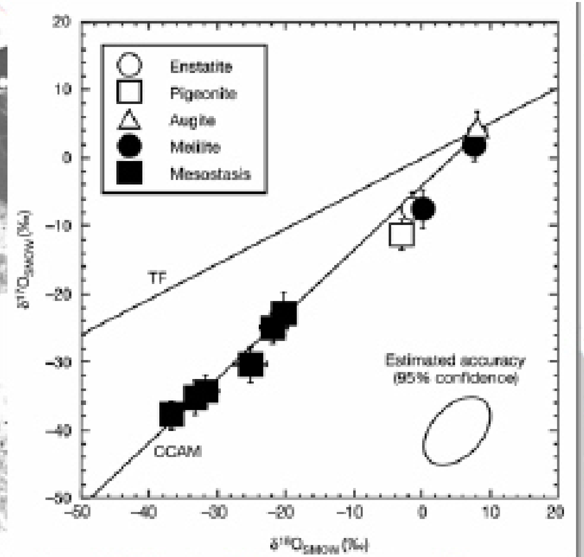

Itoh and Yurimoto (2003)

- ^{16}O-rich melt encloses ^{16}O-poor melilite.
- ^{16}O-poor → ^{16}O-rich

Evidence 4: O isotopes vs $(^{26}Al/^{26}Al)_0$

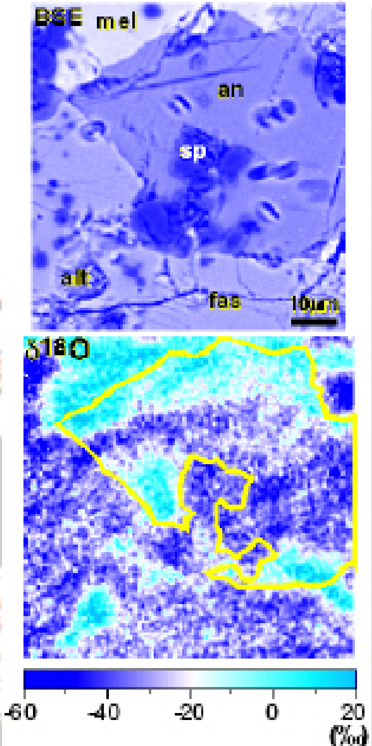

Yoshitake et al. (2005)

	^{16}O	initial ^{26}Al $\times 10^{-5}$
Sp	rich	5.1(±0.7)
Mel	poor	5.2(±1.0)
Fas	rich	4.2(±0.5)
An	rich	<0.3
An	poor	<0.3

Switching of two O-isotope reservoirs

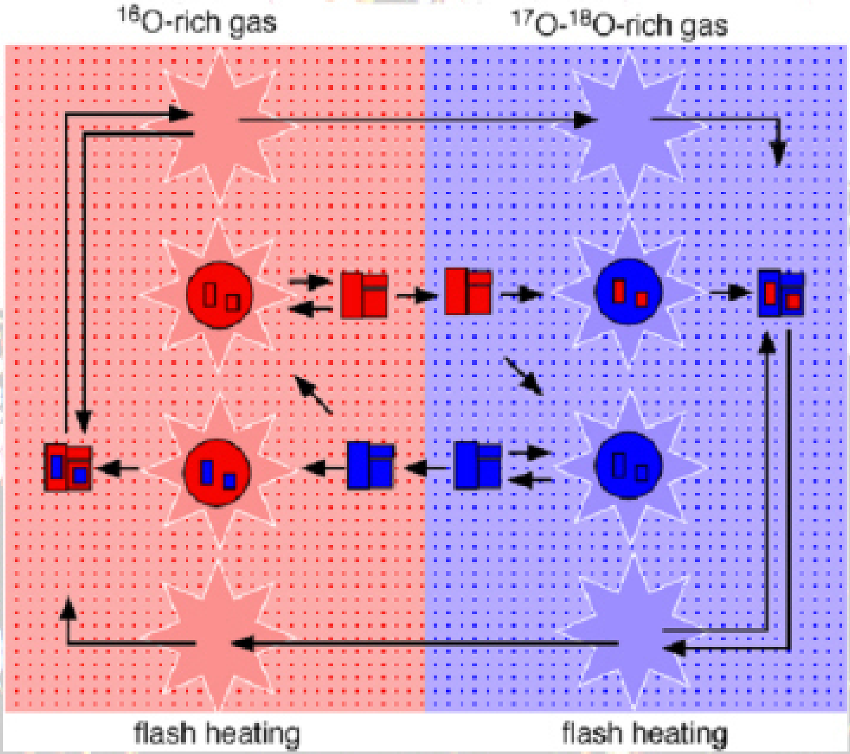

Y20a : The fragment of Coarse-grained CAI from Yamato-81020 (CO3.0) chondrite

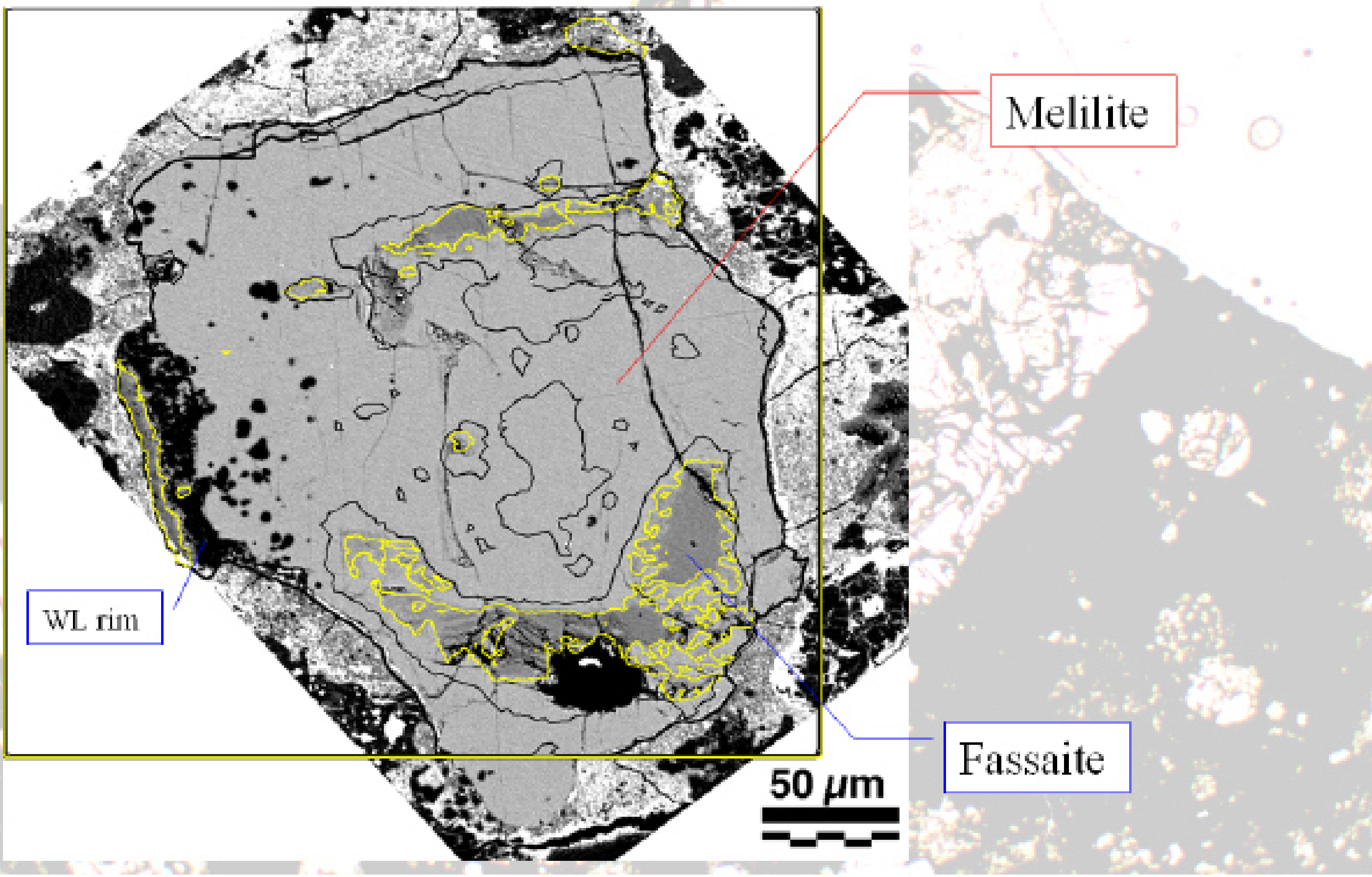

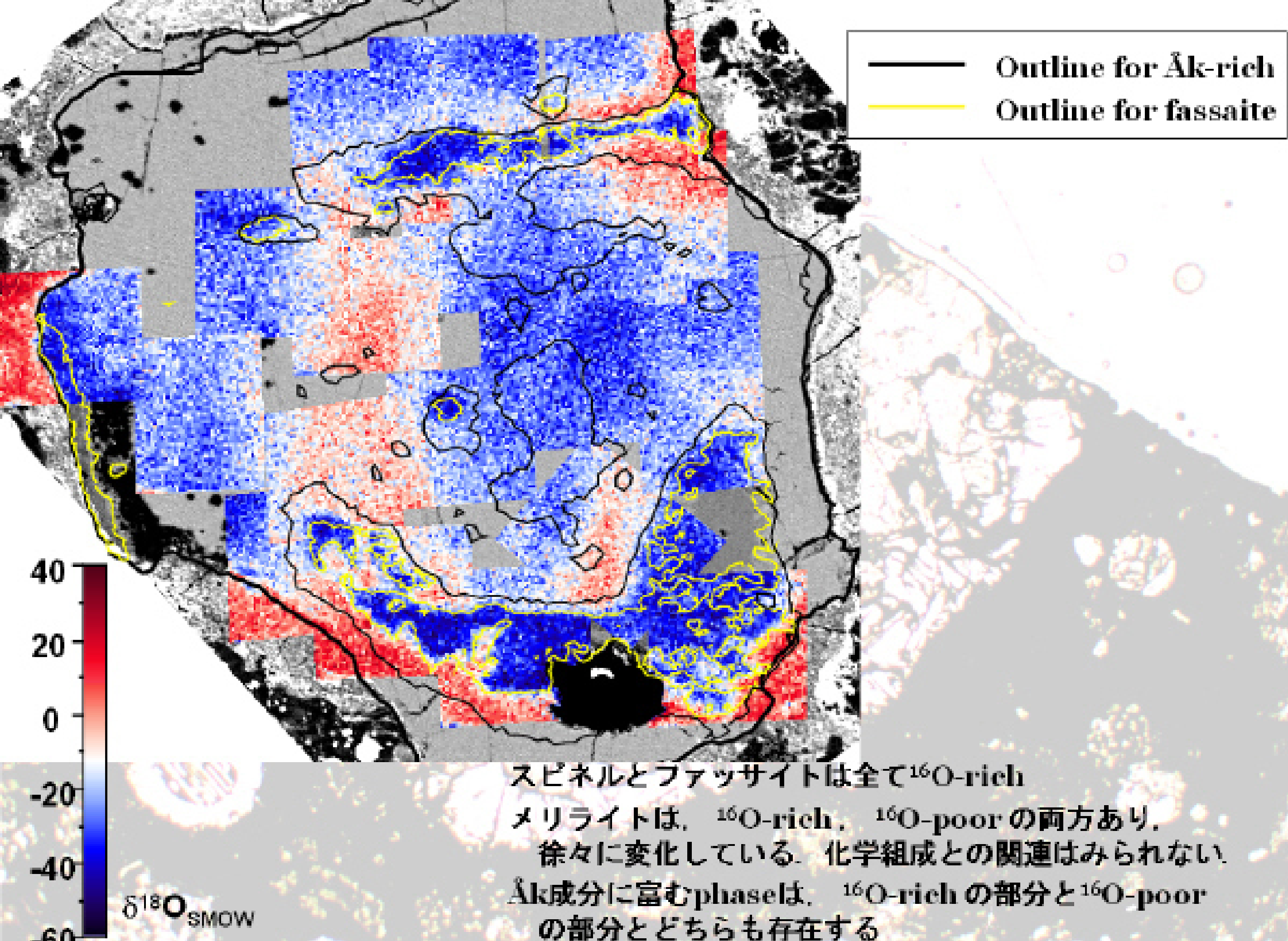

スピネルとファッサイトは全て^{16}O-rich

メリライトは，^{16}O-rich，^{16}O-poor の両方あり，
徐々に変化している．化学組成との関連はみられない．

Åk成分に富むphaseは，^{16}O-rich の部分と^{16}O-poor
の部分とどちらも存在する

Al-Mg SIMS spot of Y20a

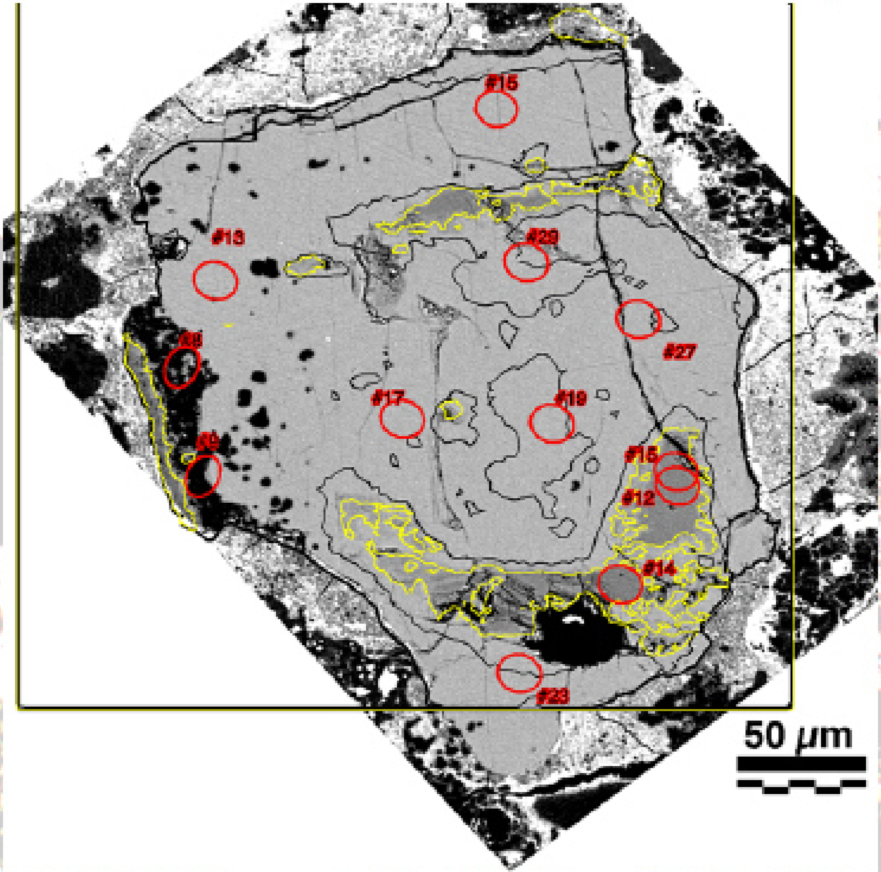

^{16}O-rich fassaite

#12, 14, 15

^{16}O-rich melilite, +Ak-glass

- 中心(interior)

#29, 19, 27

- 外側(outer)

#13, 15

^{16}O-poor melilite

#17

^{16}O-poor melilite +Ak glass

#23

^{16}O-rich WL-rim

#8, 9

Al-Mg SIMS spot of Y20a

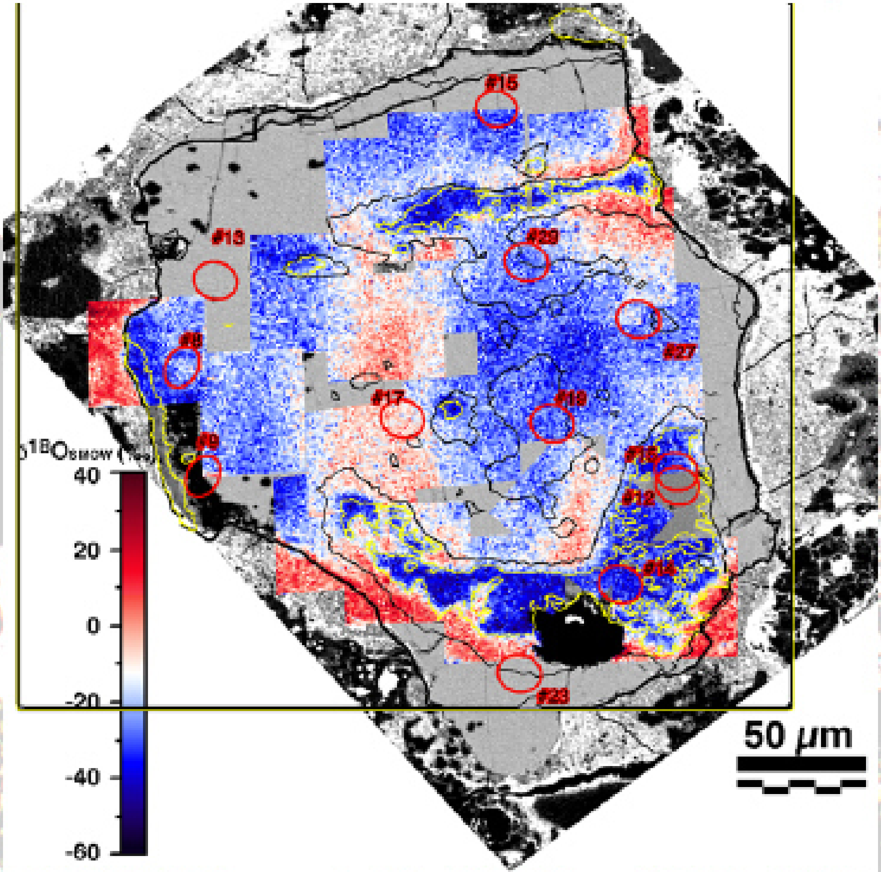

^{16}O-rich fassaite

#12, 14, 15

^{16}O-rich melilite, +Ak-glass

- 中心(interior)

#29, 19, 27

- 外側(outer)

#13, 15

^{16}O-poor melilite

#17

^{16}O-poor melilite +Ak glass

#23

^{16}O-rich WL-rim

#8, 9

Y20a Al-Mg evolution diagram Each mineral

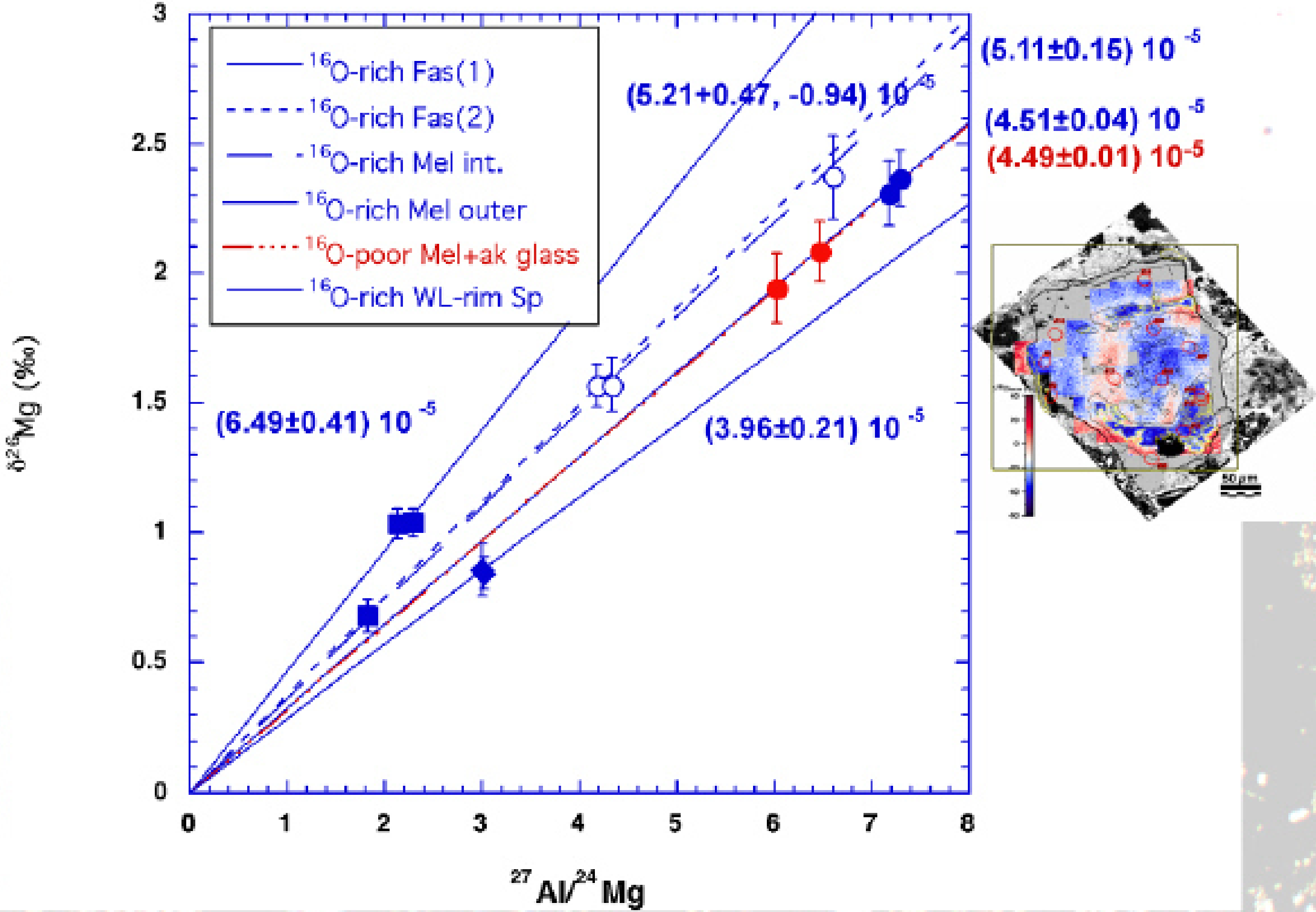

Estimation O distribution of 7R-19-1

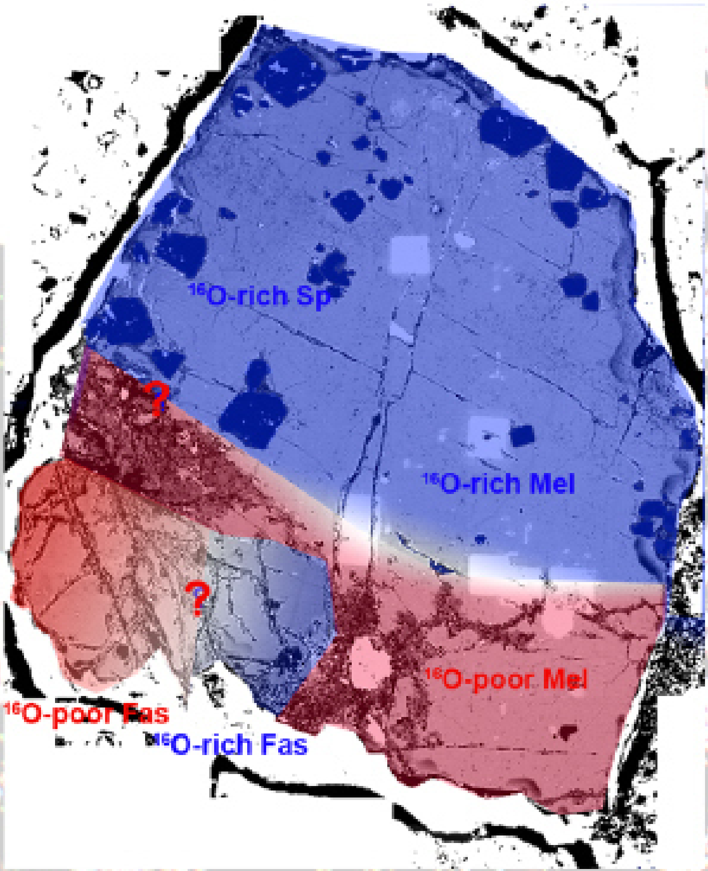

Yurimoto et al. (1998)
Ito et al. (2004)

Sharp O boundary in Mel

Also Fas has O boundary?

When these phases formed?

Estimation O distribution of 7R-19-1

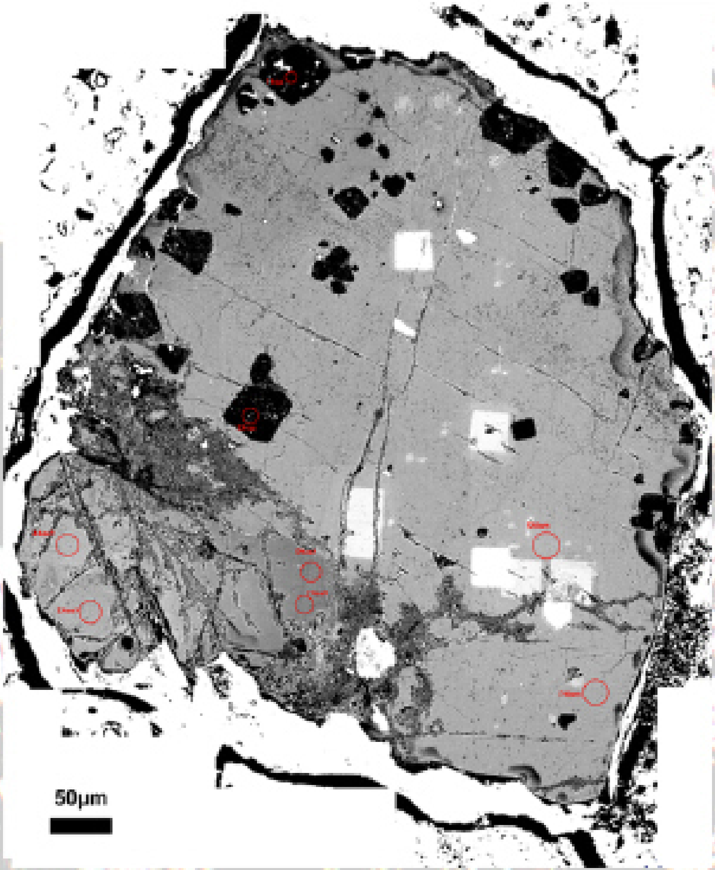

Yurimoto et al. (1998)
Ito et al. (2004)

Sharp O boundary in Mel

Also Fas has O boundary?

When these phases formed?

7R-19-1 Al-Mg evolution each mineral

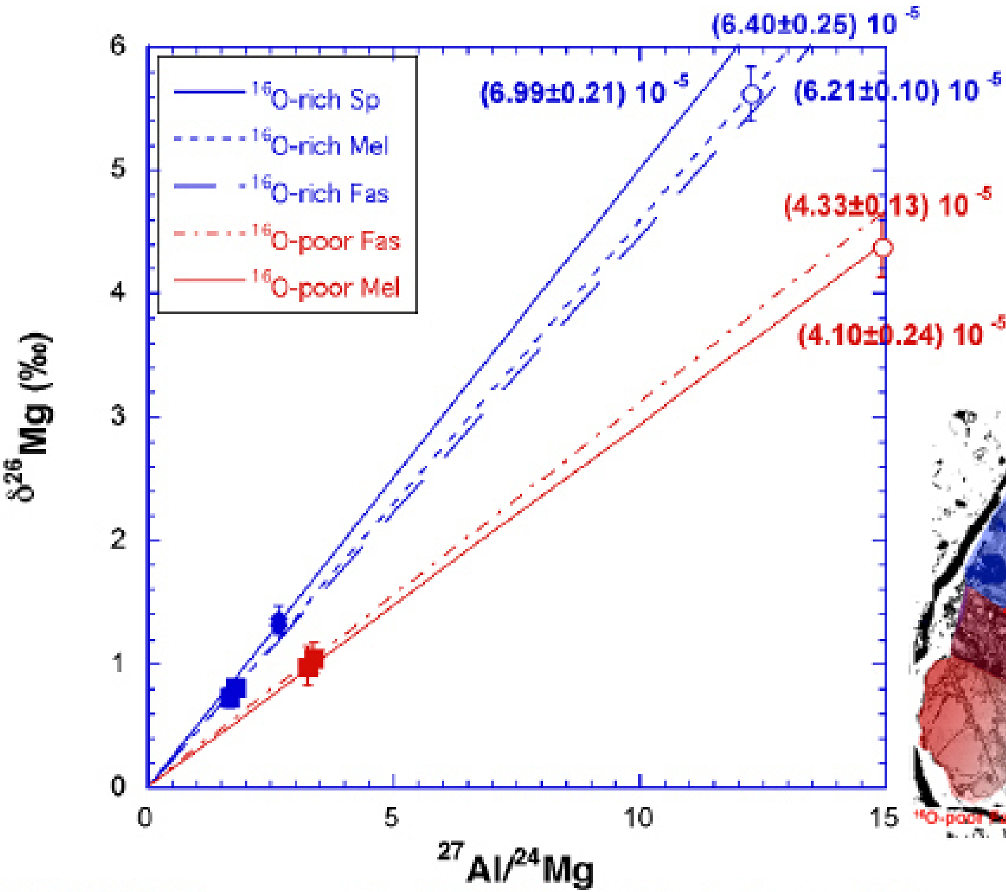

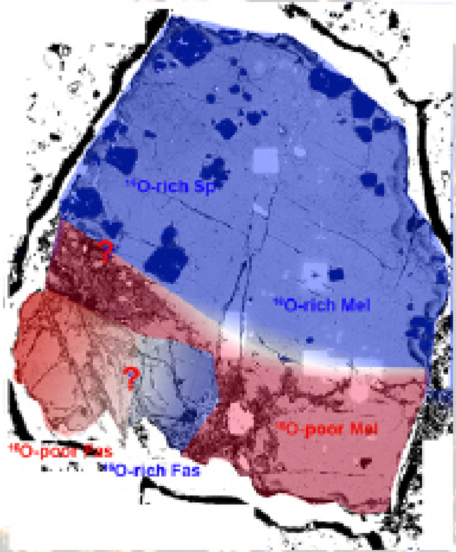

Petrography of HN3

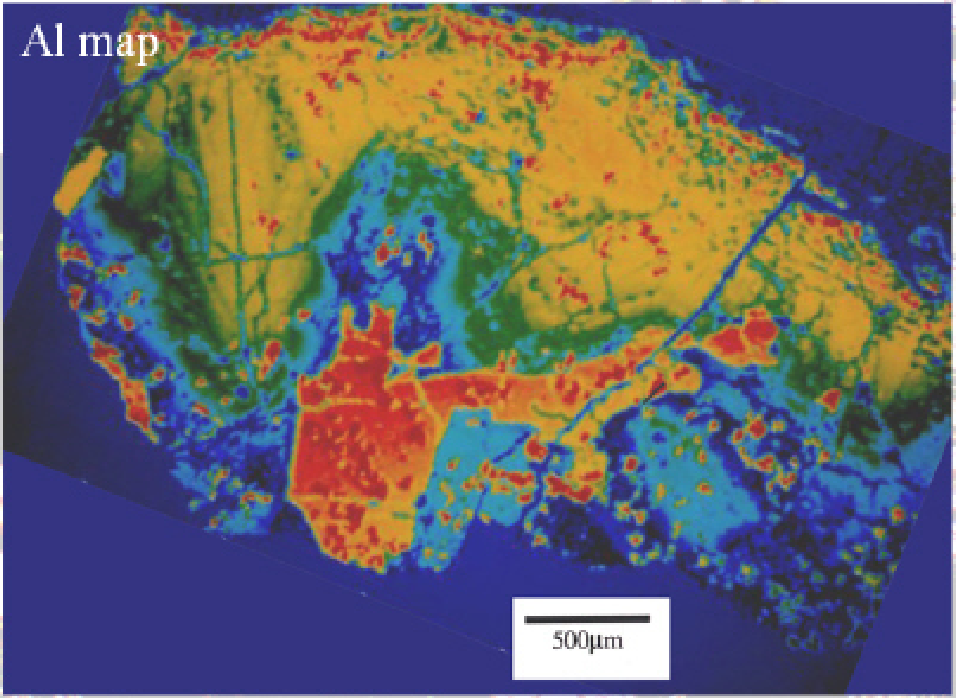

Yurimoto et al(1994)

Koike, Master thesis

Ohishi, Master thesis

Detail petrography and oxygen isotope study.

When these phases formed?

Petrography of HN3

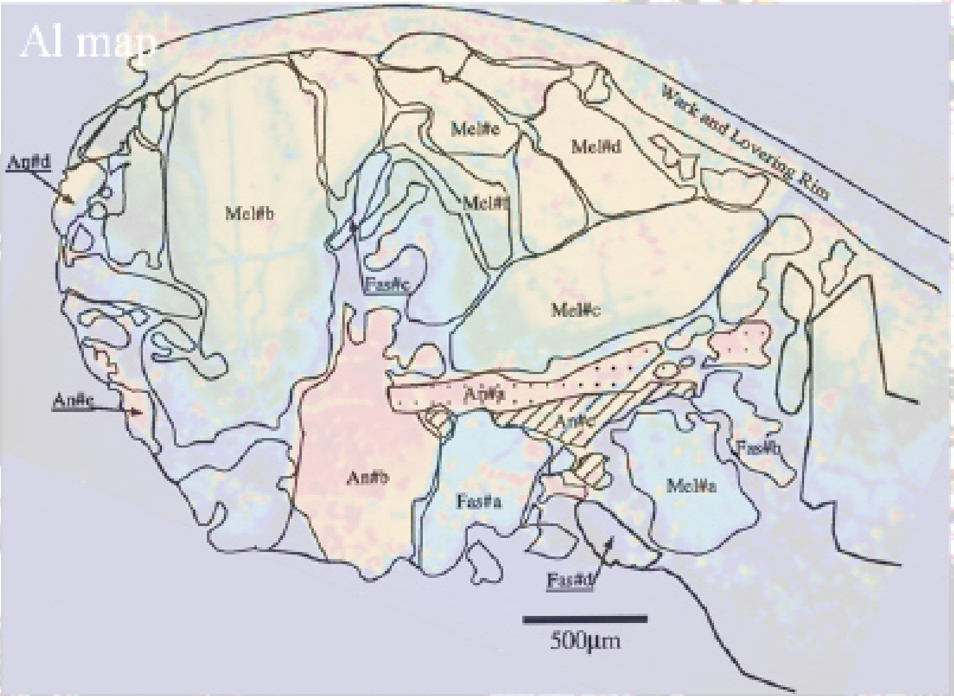

Yurimoto et al(1994)

Koike, Master thesis

Ohishi, Master thesis

Detail petrography and oxygen isotope study.

When these phases formed?

Petrography of HN3

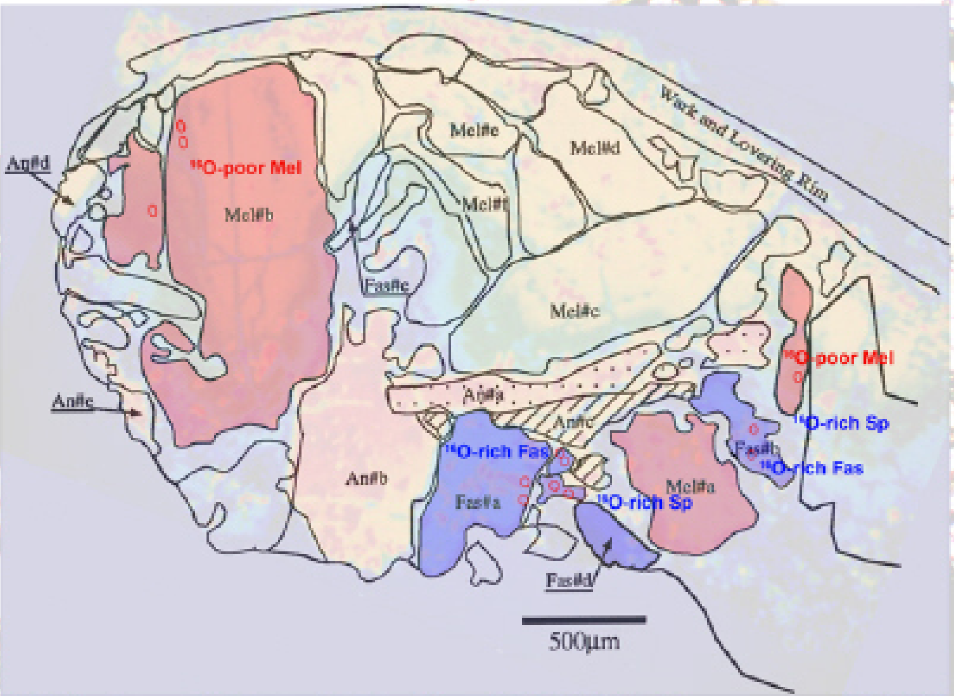

Yurimoto et al(1994)

Koike, Master thesis

Ohishi, Master thesis

Detail petrography and oxygen isotope study.

When these phases formed?

HN3 each mineral Isochron

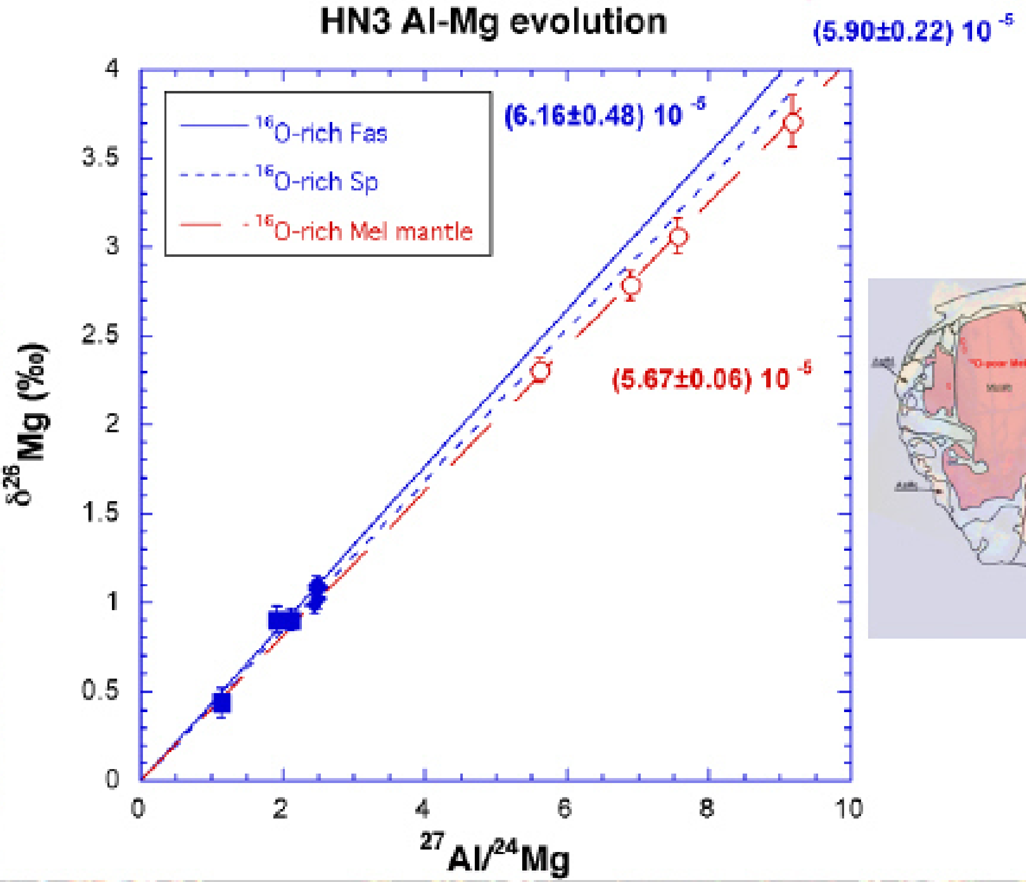

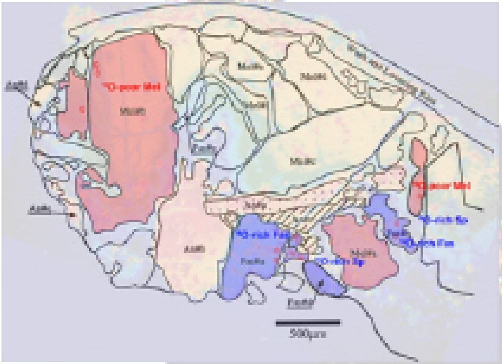

年代VS酸素同位体(粗粒CAI)

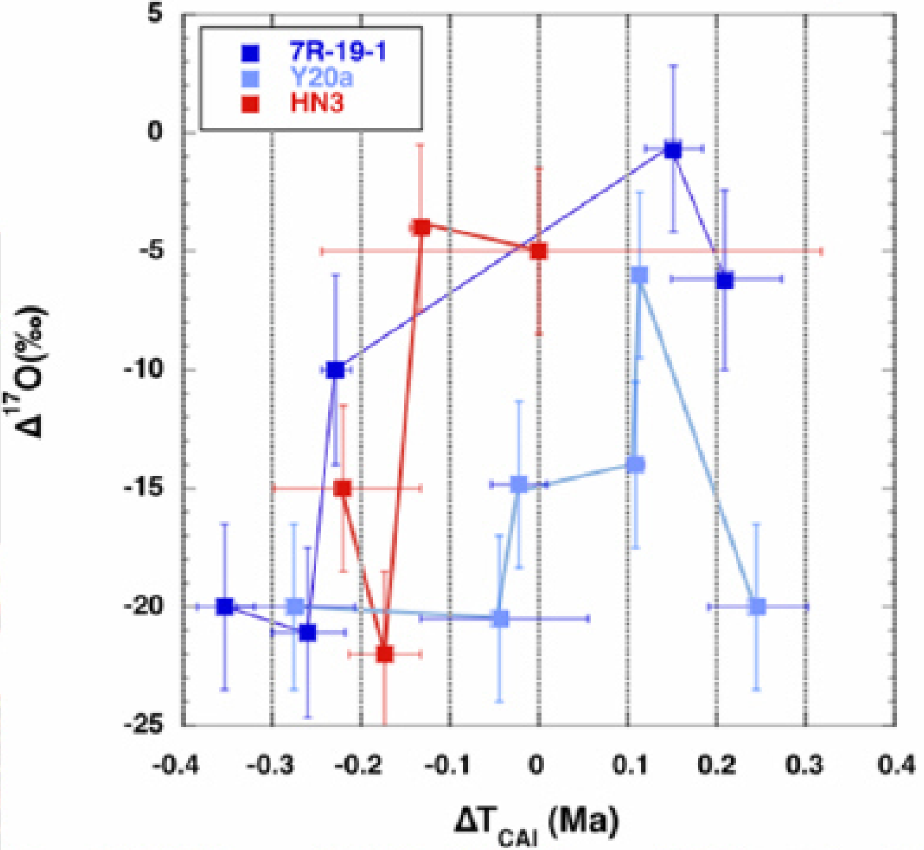

- 約60万年の間に加熱イベントが繰り返し起きた。酸素同位体変動も繰り返し起きた。
- 最初のCAI形成後少なくとも約20万年後に^{16}O-poorなリザーバが存在した。

年代VS酸素同位体(粗粒CAI)

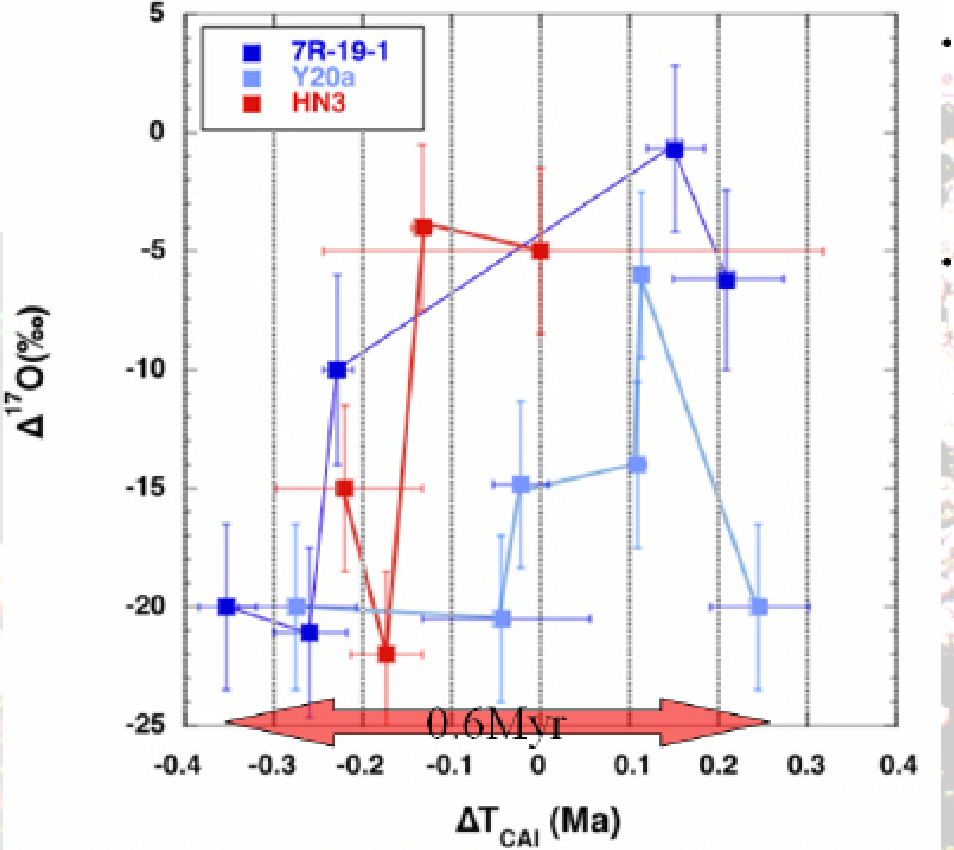

- 約60万年の間に加熱イベントが繰り返し起きた．酸素同位体変動も繰り返し起きた．
- 最初のCAI形成後少なくとも約20万年後に^{16}O-poorなリザーバが存在した．

年代VS酸素同位体（粗粒CAI）

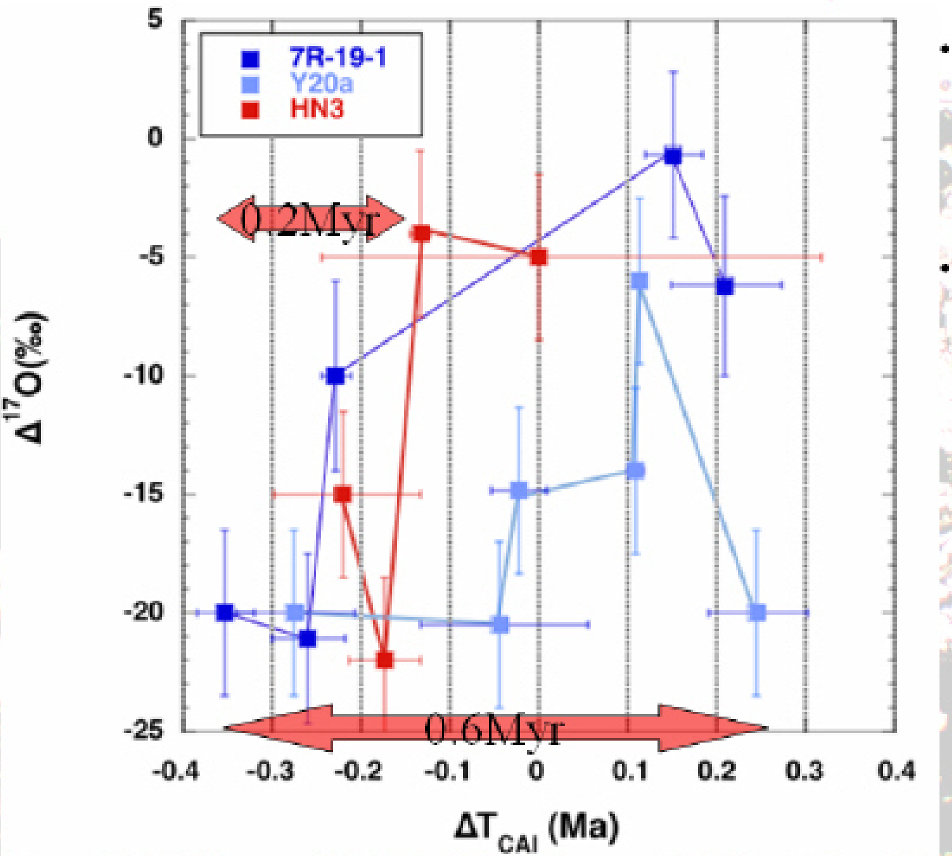

- 約60万年の間に加熱イベントが繰り返し起きた．酸素同位体変動も繰り返し起きた．
- 最初のCAI形成後少なくとも約20万年後に^{16}O-poorなリザーバが存在した．

O-isotopic compositions

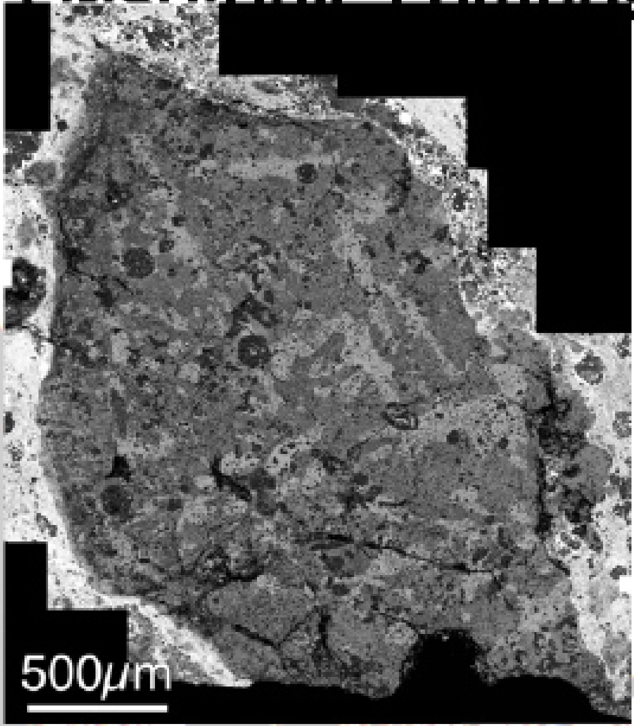

BSE image

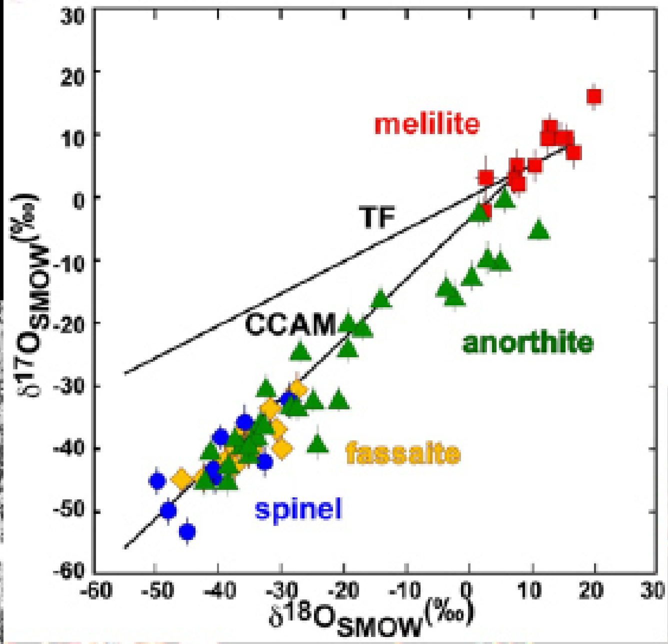

(Yoshitake et al., 2005)

O-isotopic distribution in anorthite

- A bimodal O-isotopic distribution in an anorthite
- The sharp boundary indicates that ^{16}O-poor anorthite was overgrown on the ^{16}O-rich anorthite.

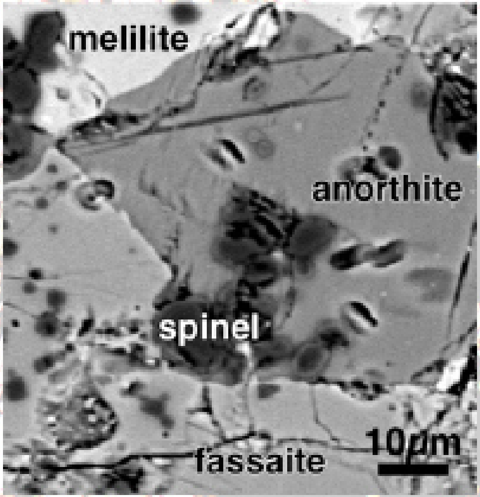

BSE image

(Nagashima et al., 2004)

O-isotopic distribution in anorthite

- A bimodal O-isotopic distribution in an anorthite
- The sharp boundary indicates that ^{16}O-poor anorthite was overgrown on the ^{16}O-rich anorthite.

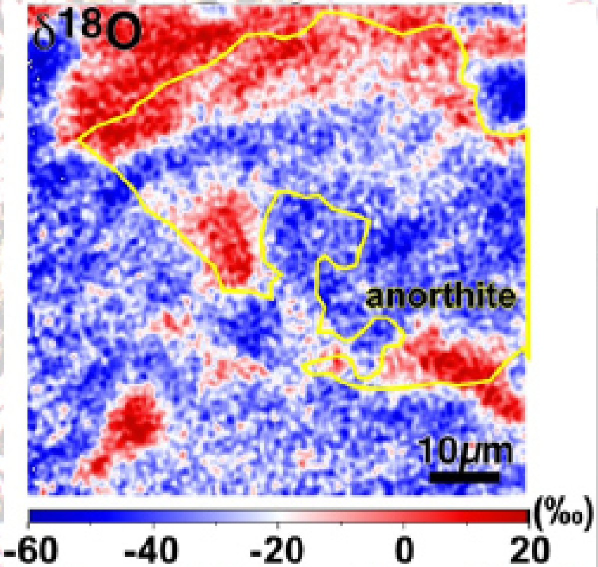

(Nagashima et al., 2004)

Results

- $(^{26}Al/^{27}Al)_0$

melilite

5.2 (±1.0) x 10^{-5} (2σ)

spinel

5.1 (±0.7) x 10^{-5} (2σ)

fassaite

4.2 (±0.5) x 10^{-5} (2σ)

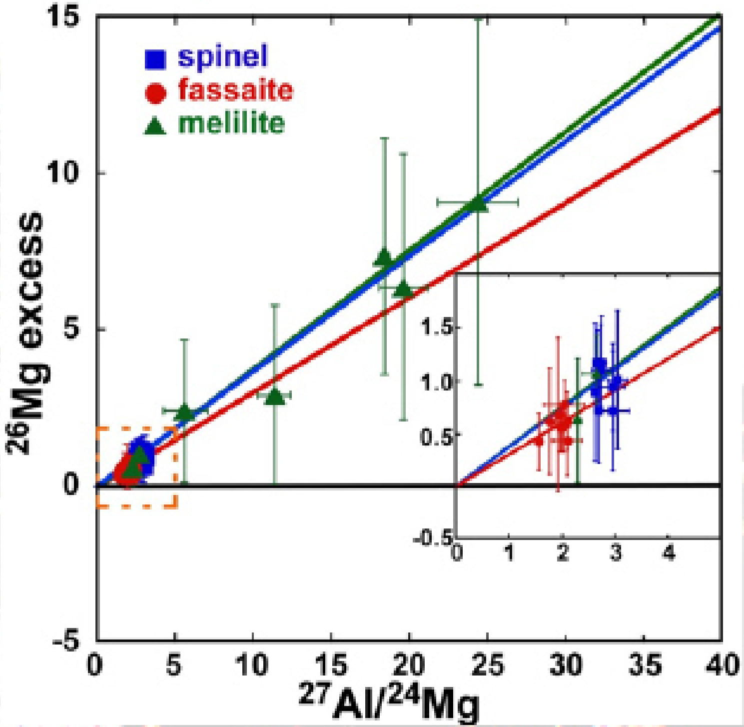

Results

- $(^{26}Al/^{27}Al)_0$

melilite

5.2 (±1.0) x 10^{-5} (2σ)

spinel

5.1 (±0.7) x 10^{-5} (2σ)

fassaite

4.2 (±0.5) x 10^{-5} (2σ)

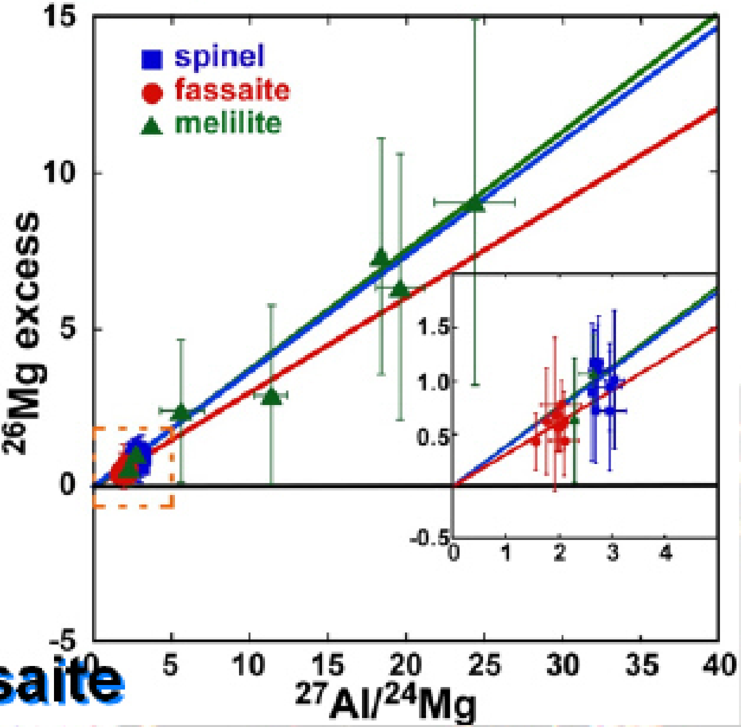

melilite+spinel+fassaite

4.7 (±0.4) x 10^{-5} (2σ)

Results

- $(^{26}Al/^{27}Al)_0$

melilite+spinel+fassaite

4.7 (±0.4) x 10^{-5} (2σ)

anorthite

-0.4 (±3.5) x 10^{-6} (2σ)

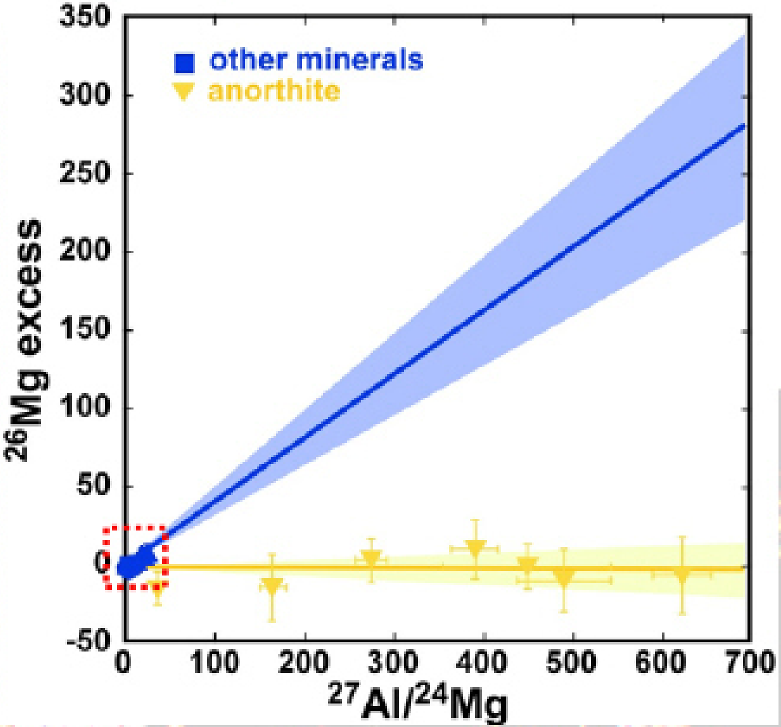

Results

- $(^{26}Al/^{27}Al)_0$

melilite+spinel+fassaite

4.7 (±0.4) x 10^{-5} (2σ)

anorthite

-0.4 (±3.5) x 10^{-6} (2σ)

Homogeneous distribution of Mg isotopes

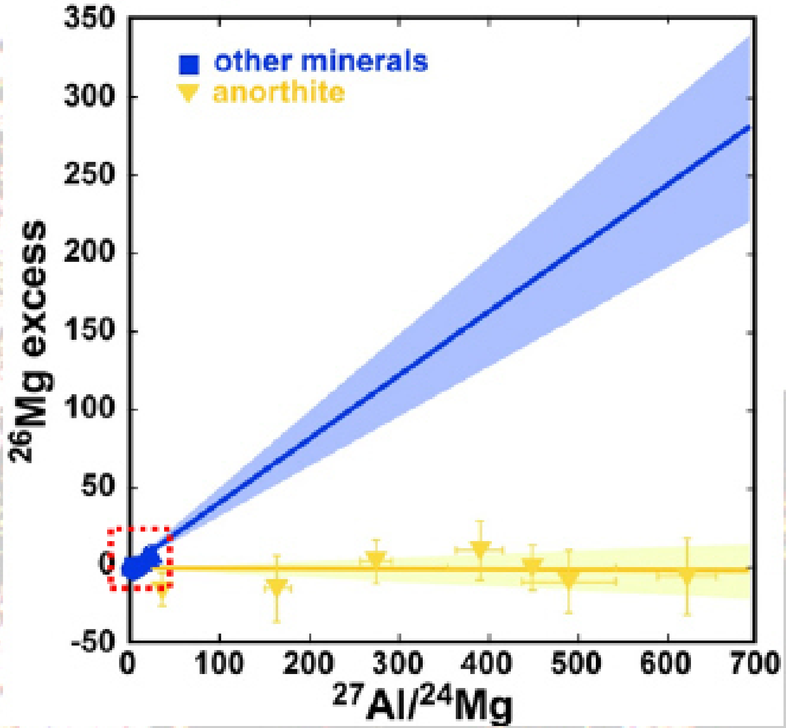

O & Mg isotopes in anorthite

Homogeneous distribution of Mg isotopes

Heterogeneous distribution of O isotopes

There is no correlation between O and Mg isotopic compositions.

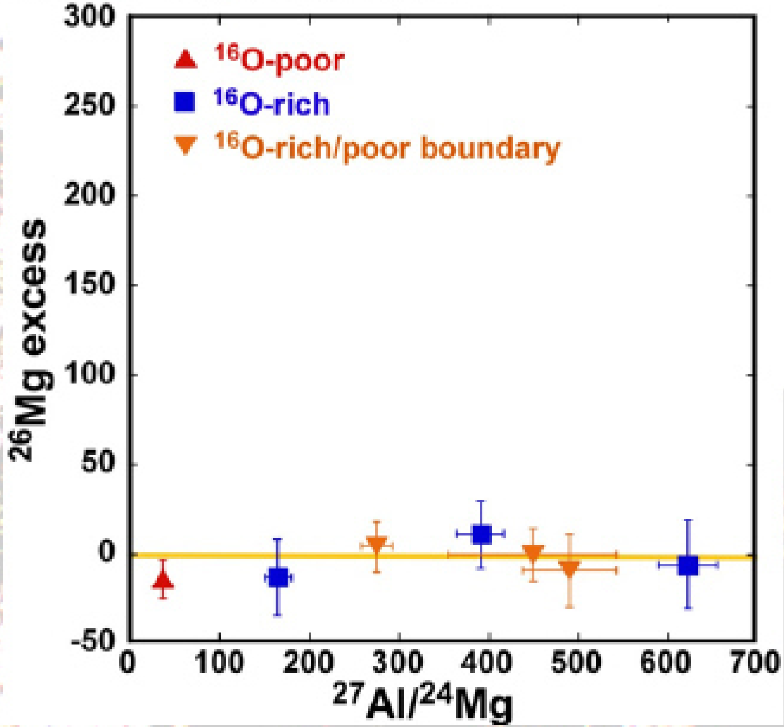

原始太陽系円盤ガスの酸素同位体変動

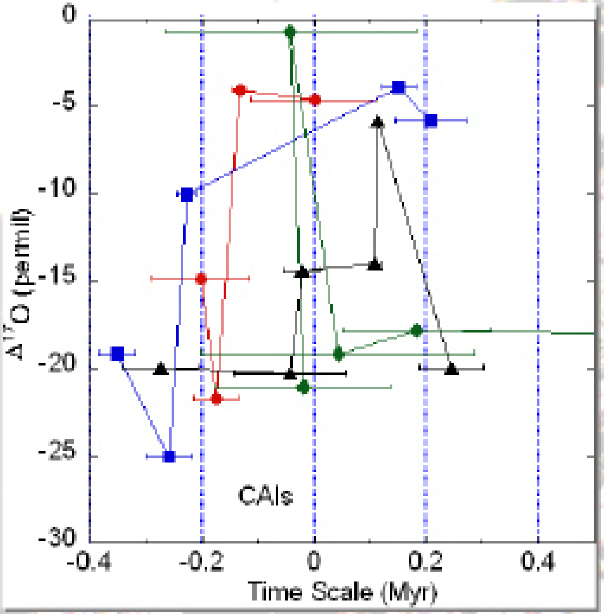

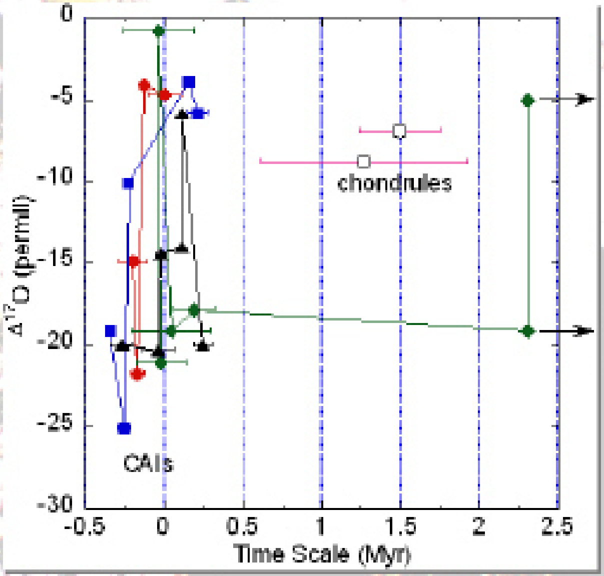

- １個のCAIの形成期間（一瞬〜数百万年）
- １個のCAI周辺の円盤ガスは10万年より短い間に異なる酸素同位体比をもつものに切り替わる。
- 酸素同位体比の切り替わり現象は数百万年間起きている。

原始太陽系円盤ガスの酸素同位体変動

巻出健太郎，吉武美和，伊藤正一

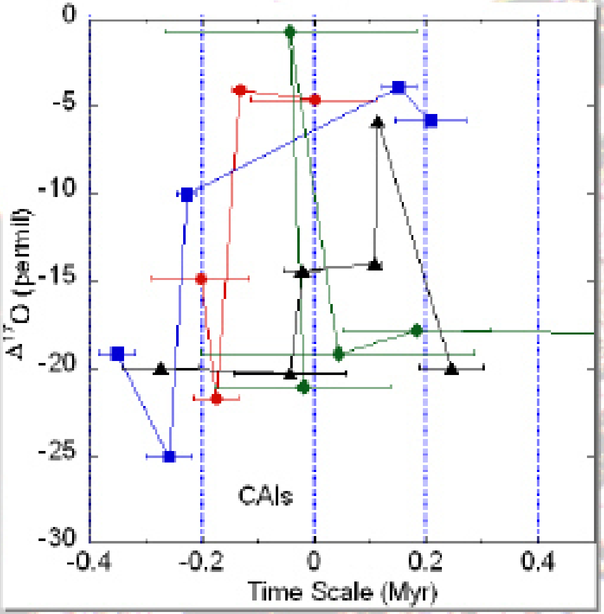

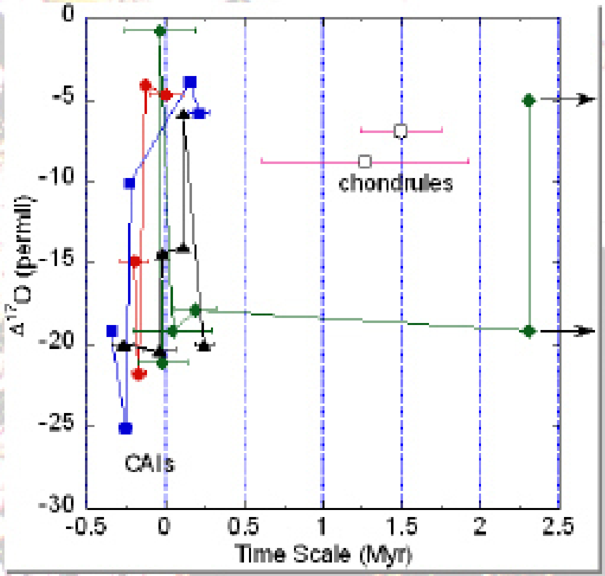

- １個のCAIの形成期間（一瞬～数百万年）
- １個のCAI周辺の円盤ガスは10万年より短い間に異なる酸素同位体比をもつものに切り替わる。
- 酸素同位体比の切り替わり現象は数百万年間起きている。

Chondruleの酸素同位体

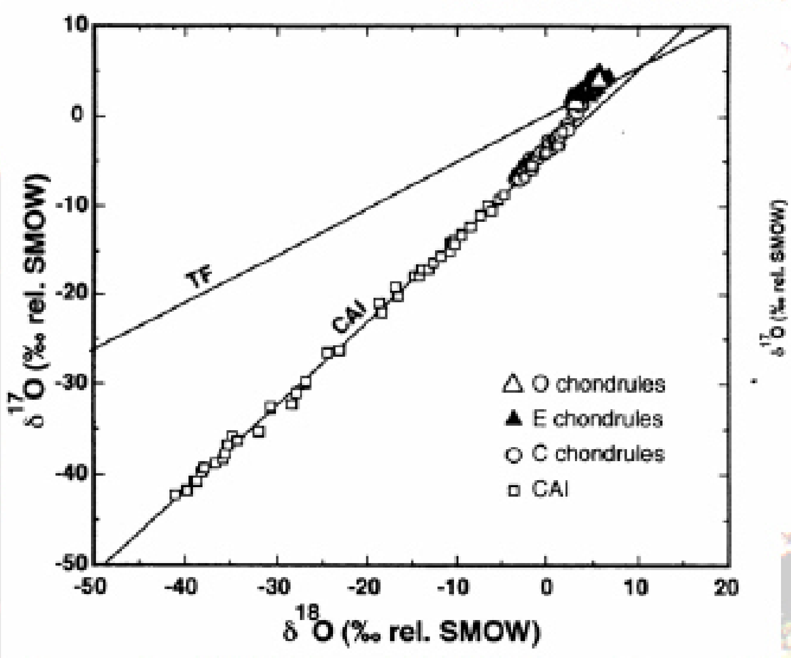

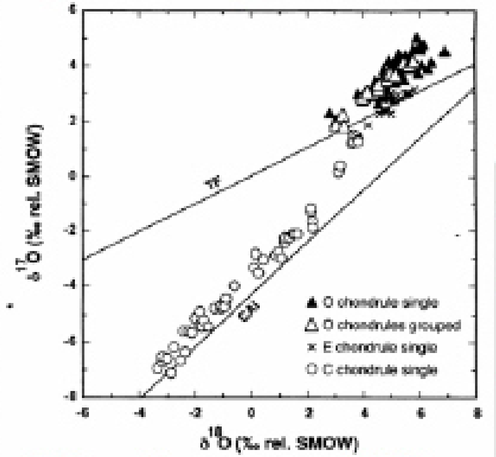

Clayton (1993)

Chondruleの酸素同位体

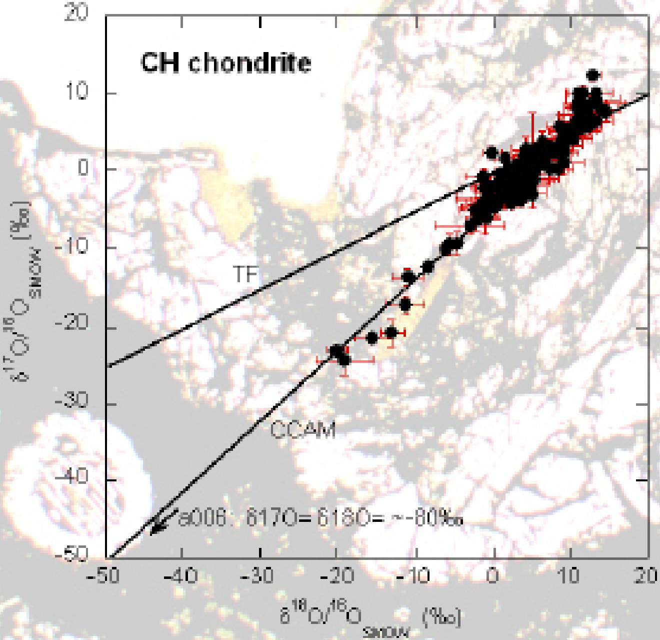

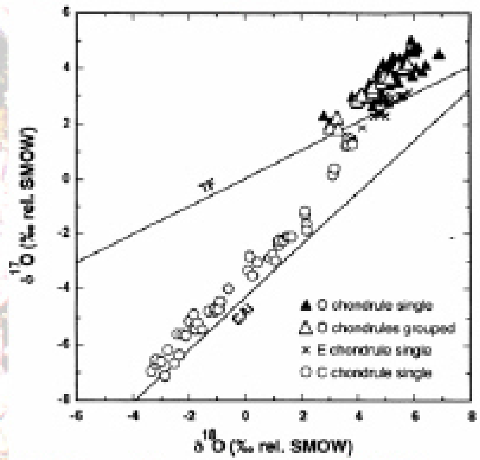

Acfer 214 CH chondrite

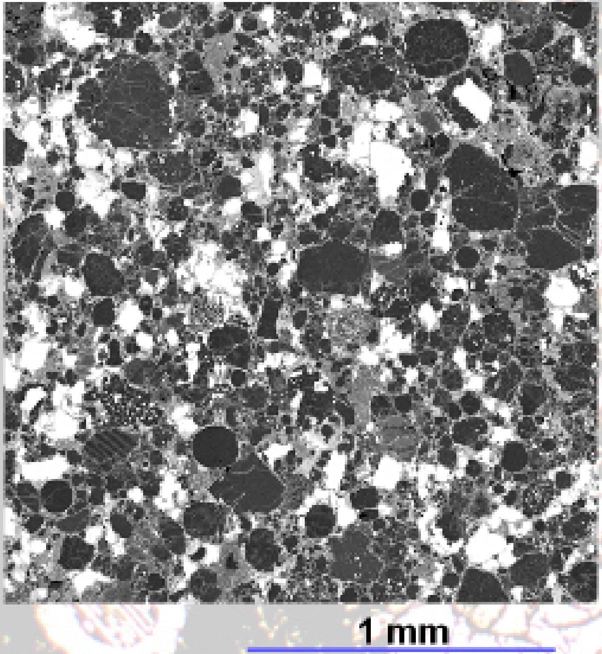

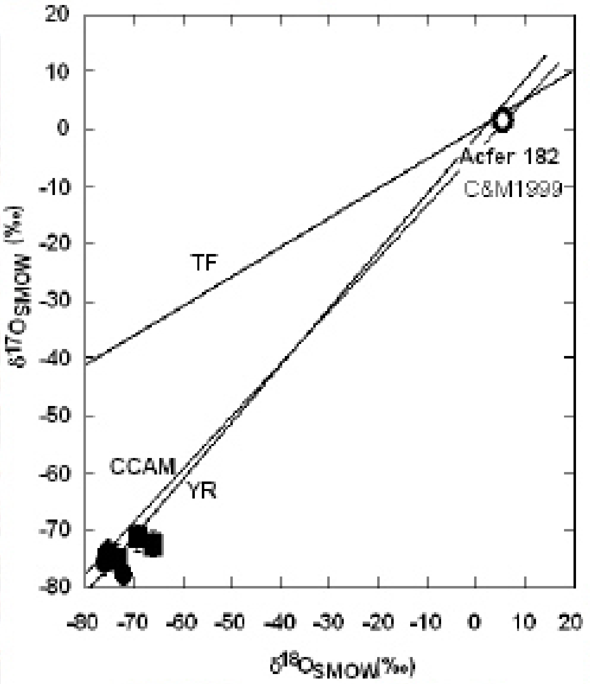

a006–texture & O isotope

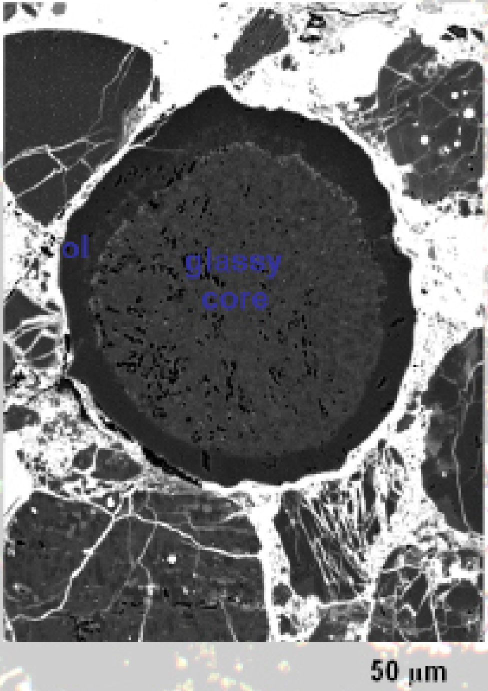

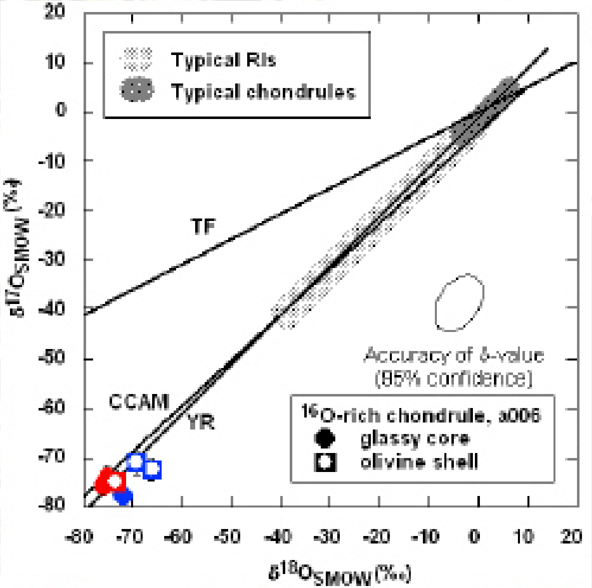

a006–Mg, Si & O isotopes

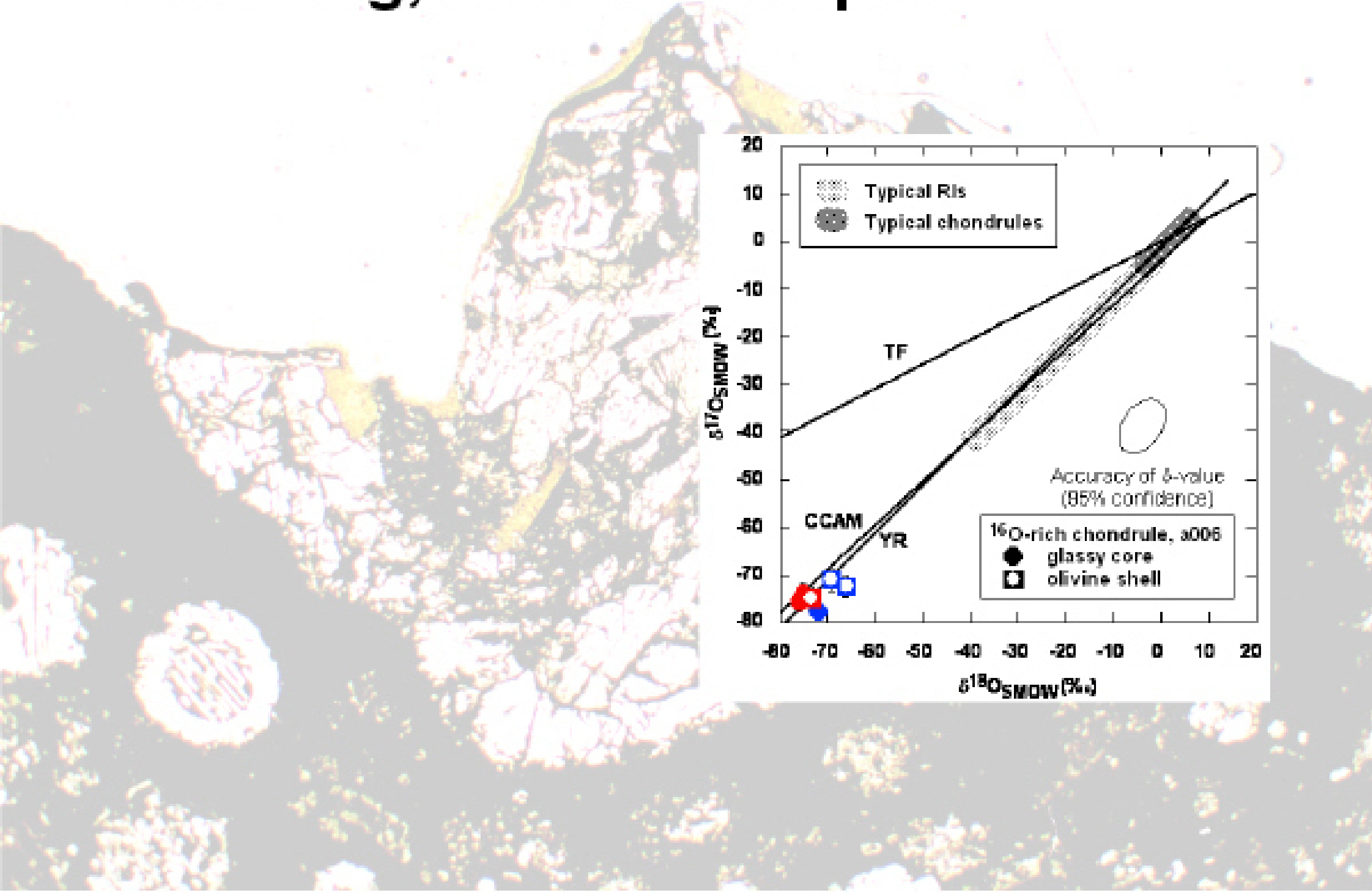

a006–Mg, Si & O isotopes

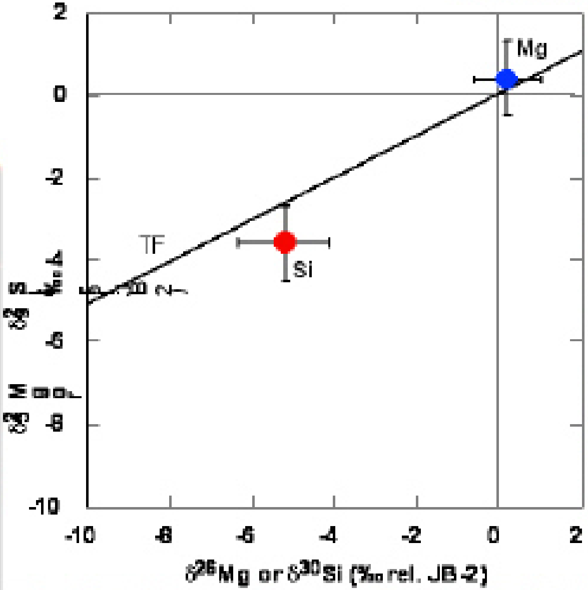

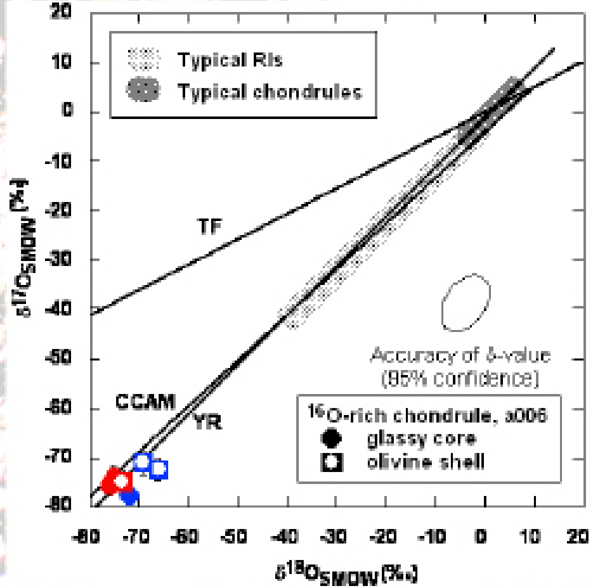

a006–bulk composition

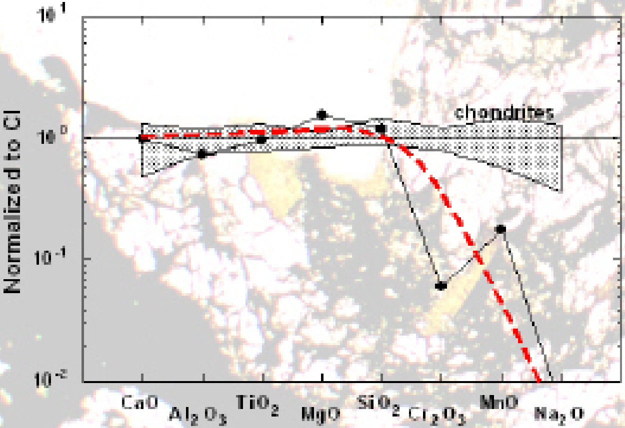

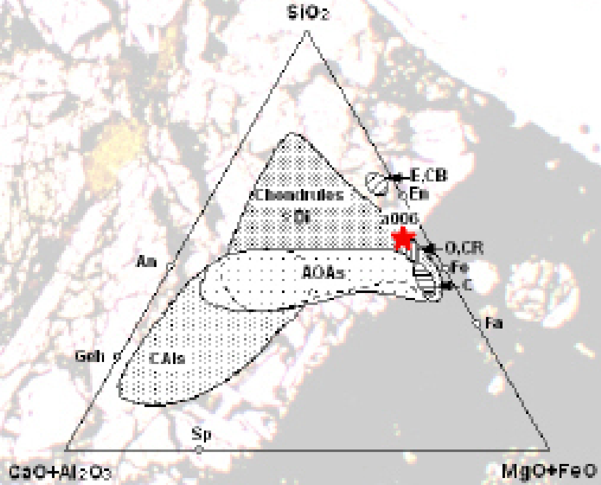

a006 vs other CC & CAIs in Acfer 214

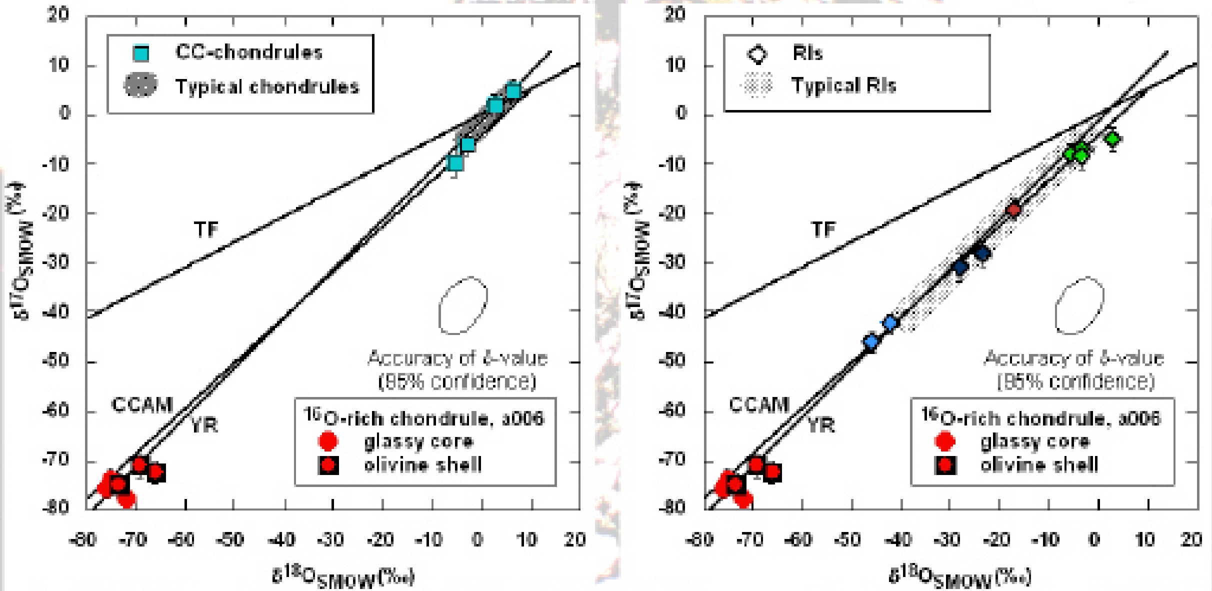

コンドリュールの形成条件

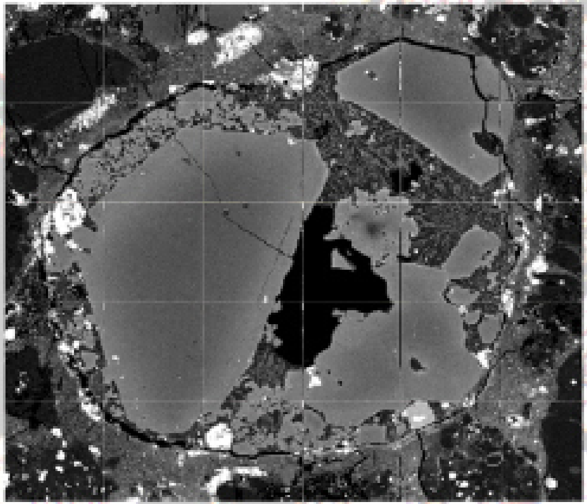

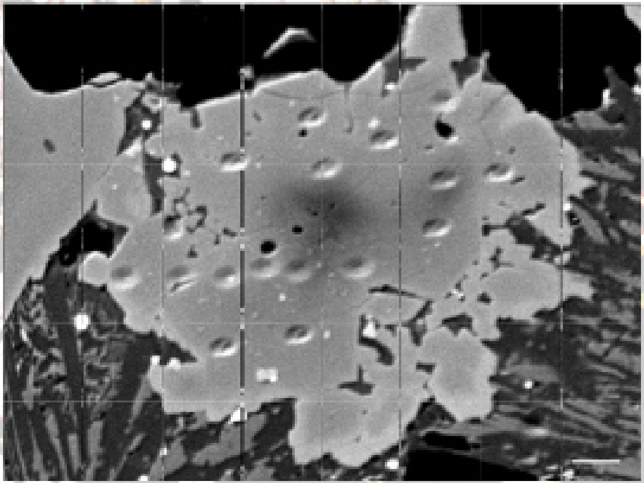

コンドリュールの形成条件

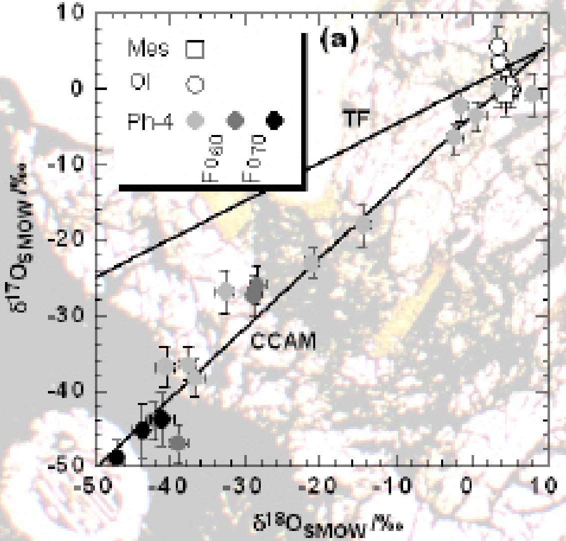

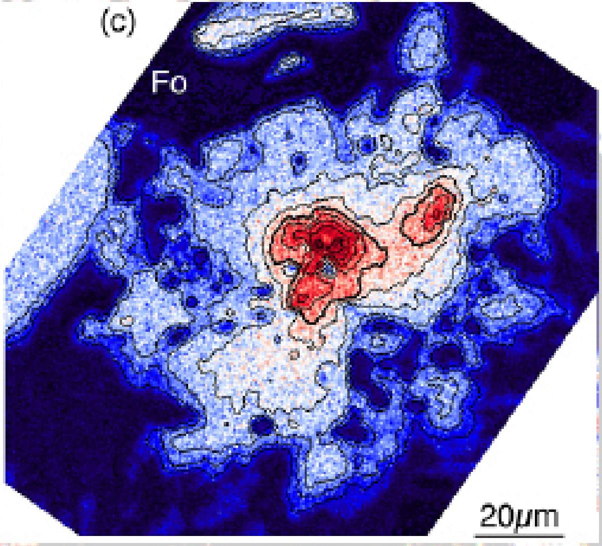

Sp bearing chondrules

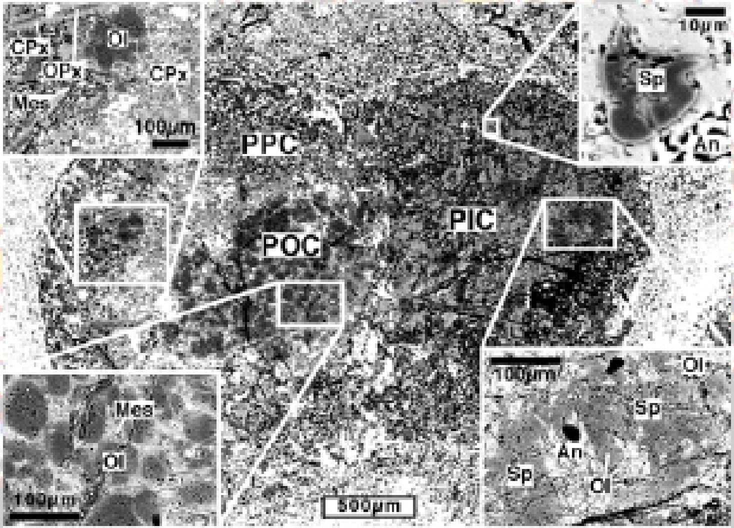

Maruyama et al.

Fig.2

酸素同位体

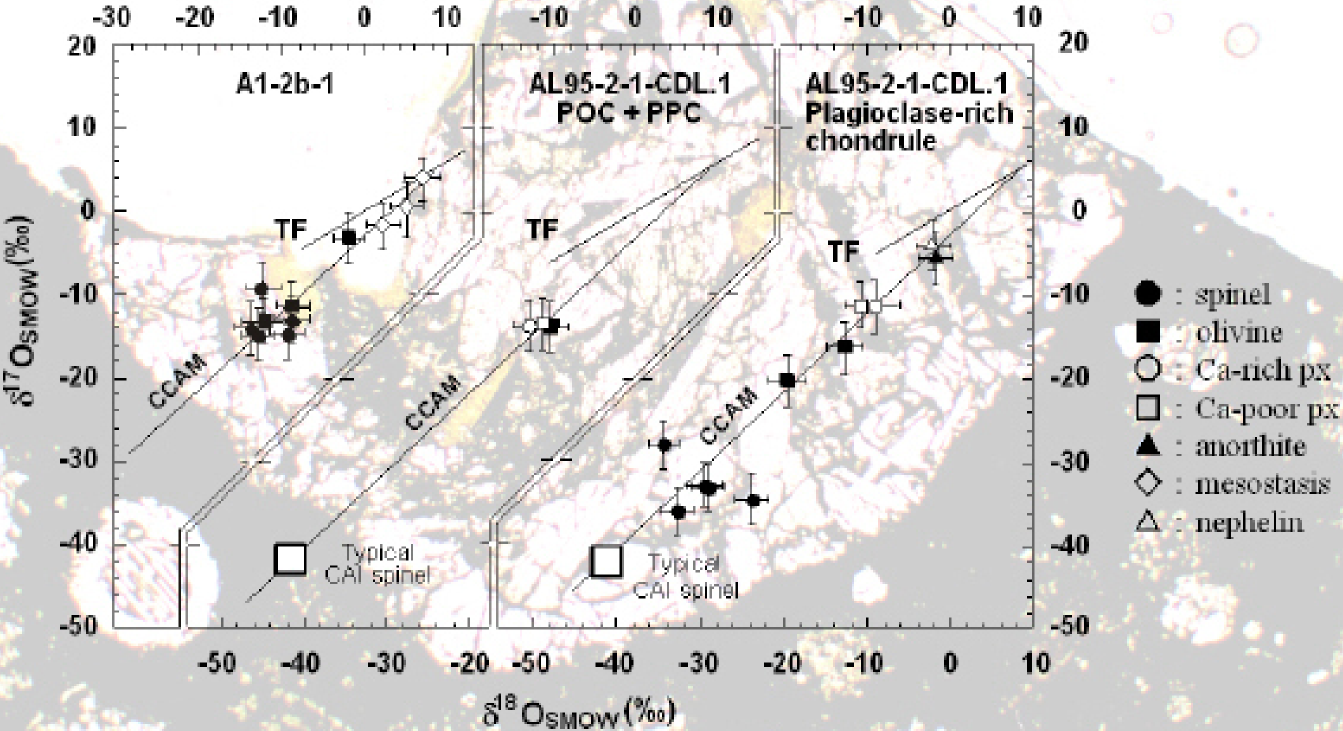
A1-2b-1
AL95-2-1-CDL.1
POC + PPC
AL95-2-1-CDL.1
Plagioclase-rich
chondrule
TF
CCAM
Typical
CAI spinel
δ17OSMOW(‰)
δ18OSMOW(‰)
-30 -20 -10 0 10
-10 0 10
-10 0 10
20 10 0 -10 -20 -30 -40 -50
-50 -40 -30 -20 -50 -40 -30 -20 -10 0 10
: spinel
: olivine
: Ca-rich px
: Ca-poor px
: anorthite
: mesostasis
: nephelin

Allende 隕石中の２つのコンドリュールの反射電子像図

Chapter 3: BSE(Allende chondrules)

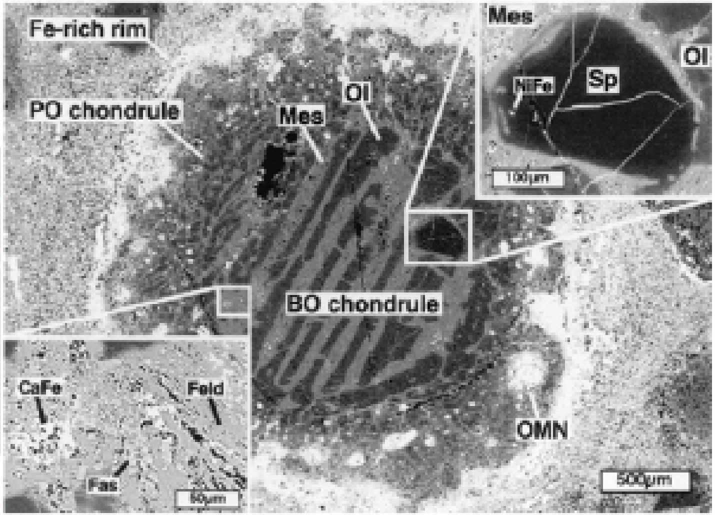

Fig. A1 バードオリビンコンドリュールの反射電子像図（Maruyama et al.,　2003)

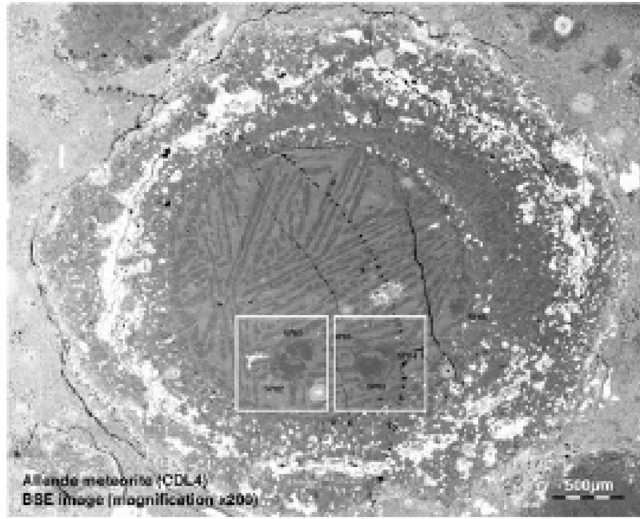

Fig. CDL4 バードオリビンコンドリュールの反射電子像図

A1　　　　**CDL4**

Results~ Allende 隕石中のスピネルの酸素同位体組成

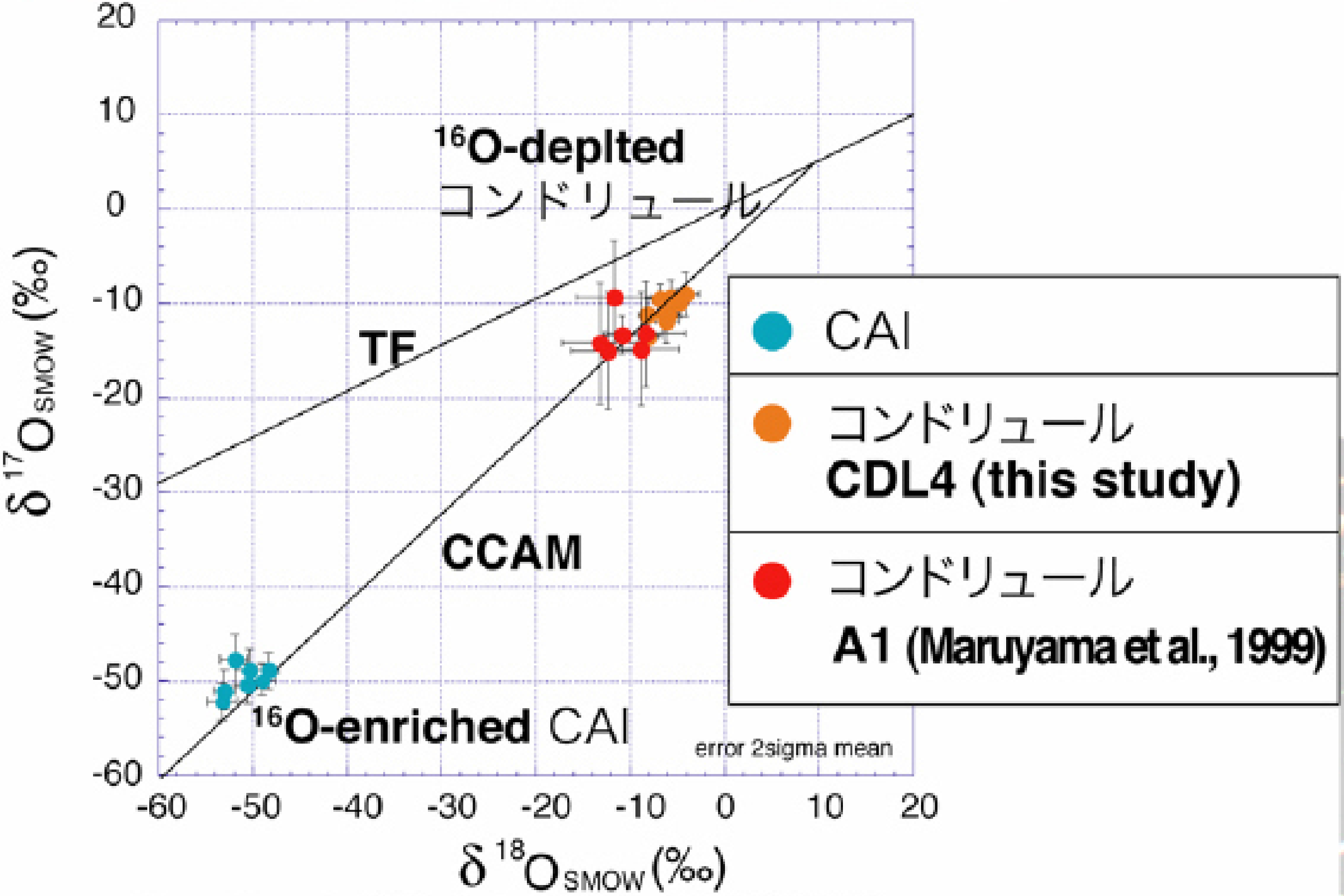

Fig. Allende隕石中のスピネルの酸素同位体

Results (Mg isotope for A1 コンドリュール)

Chapter 3: CAIs and chondrules from Allende CV-chondrite

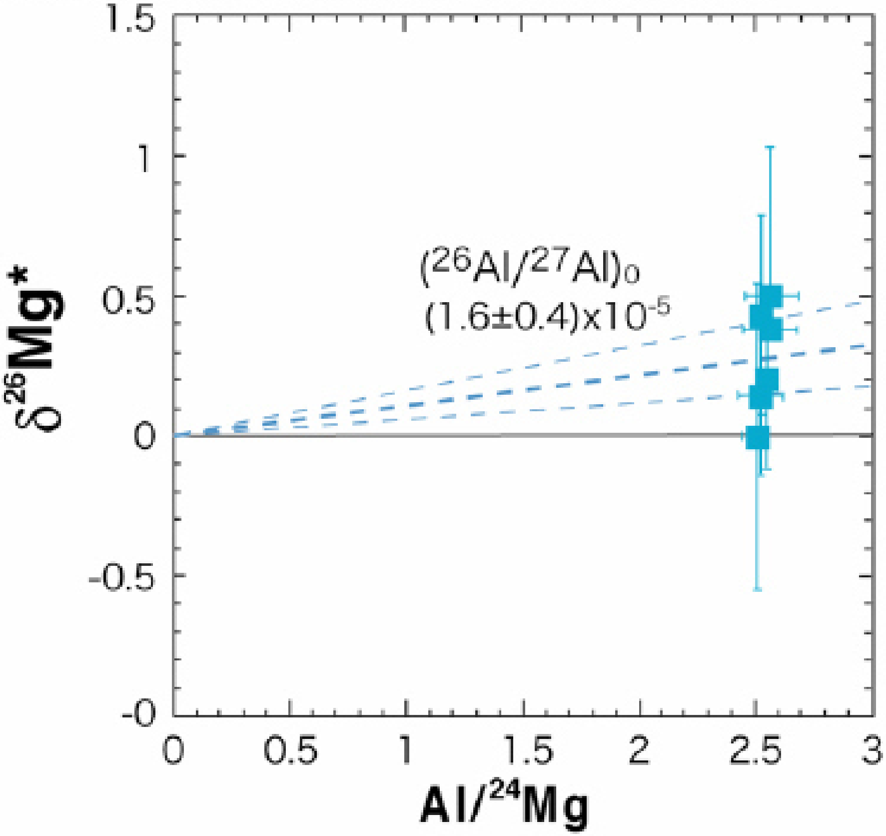

δ26Mg* の過剰あり

A1 コンドリュール中のスピネルの Al-Mg system

Results (Mg isotope for CDL4 コンドリュール)

Chapter 3: CAIs and chondrules from Allende CV-chondrite

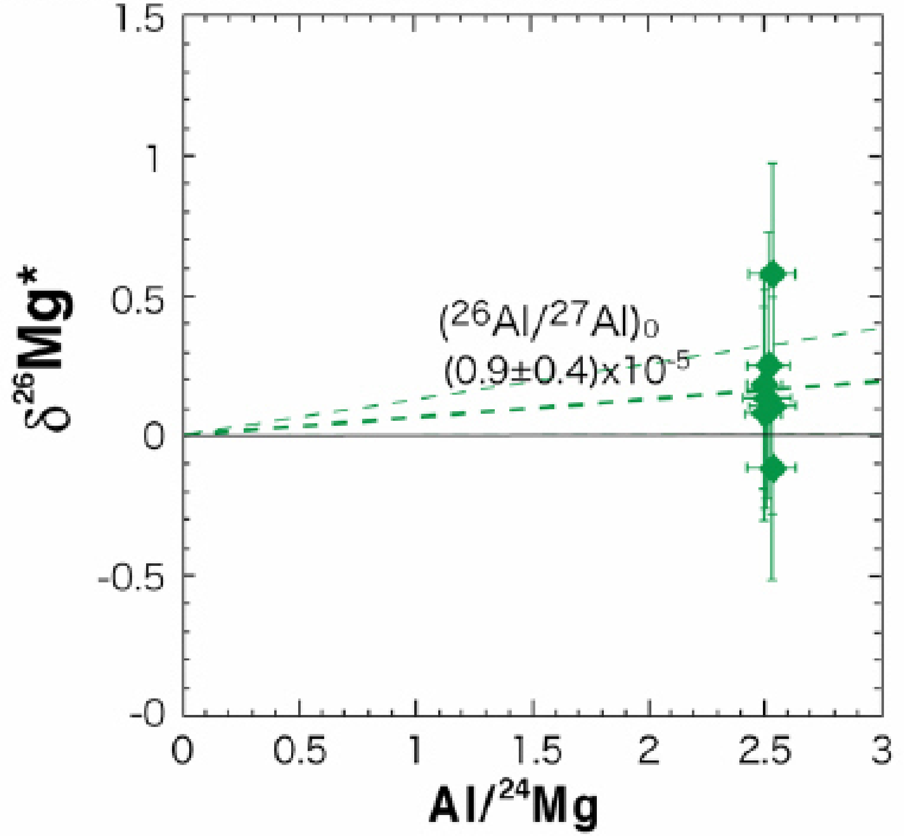

δ26Mg* の過剰あり

- CDL4 コンドリュール中のスピネルの Al-Mg

Results

Chapter 3: CAIs and condrules from Allende CV-chondrite

*($^{26}Al/^{27}Al)_0=4.5x10^{-5}$
を時刻０として

スピネル	酸素同位体	$(^{26}Al/^{27}Al)_0$	ΔT*
CAI	**^{16}O-enriched**	$(7.3\pm0.5)x10^{-5}$	$-0.5^{-0.1}_{+0.1}$ **Myr**
コンドリュール A1	**^{16}O-depleted**	$(1.6\pm0.4)x10^{-5}$	$1.1^{+0.2}_{-0.2}$ **Myr**
コンドリュール CDL	**^{16}O-depleted**	$(0.9\pm0.4)x10^{-5}$	$1.7^{+0.7}_{-0.4}$ **Myr**

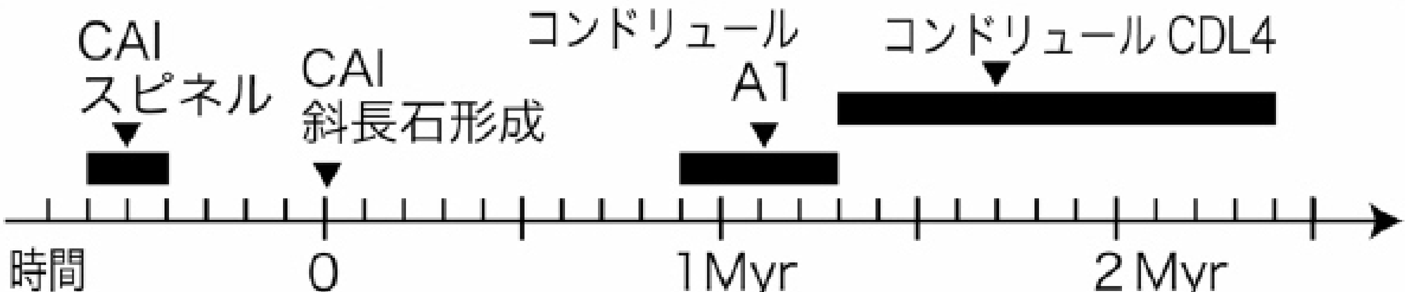

Petrography of C1m (Enveloping compound chondrule)

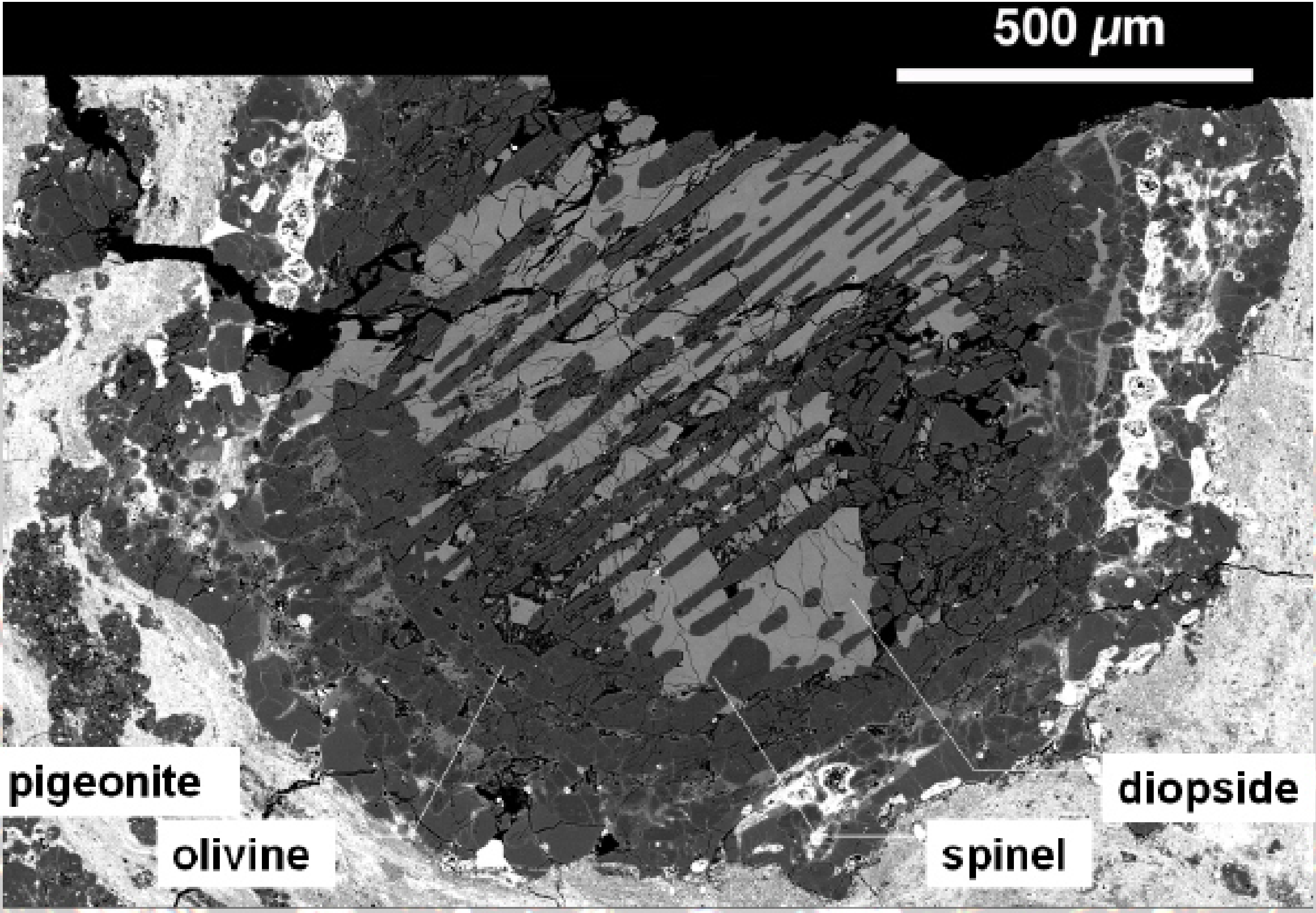

Petrography of C1m (Enveloping compound chondrule)

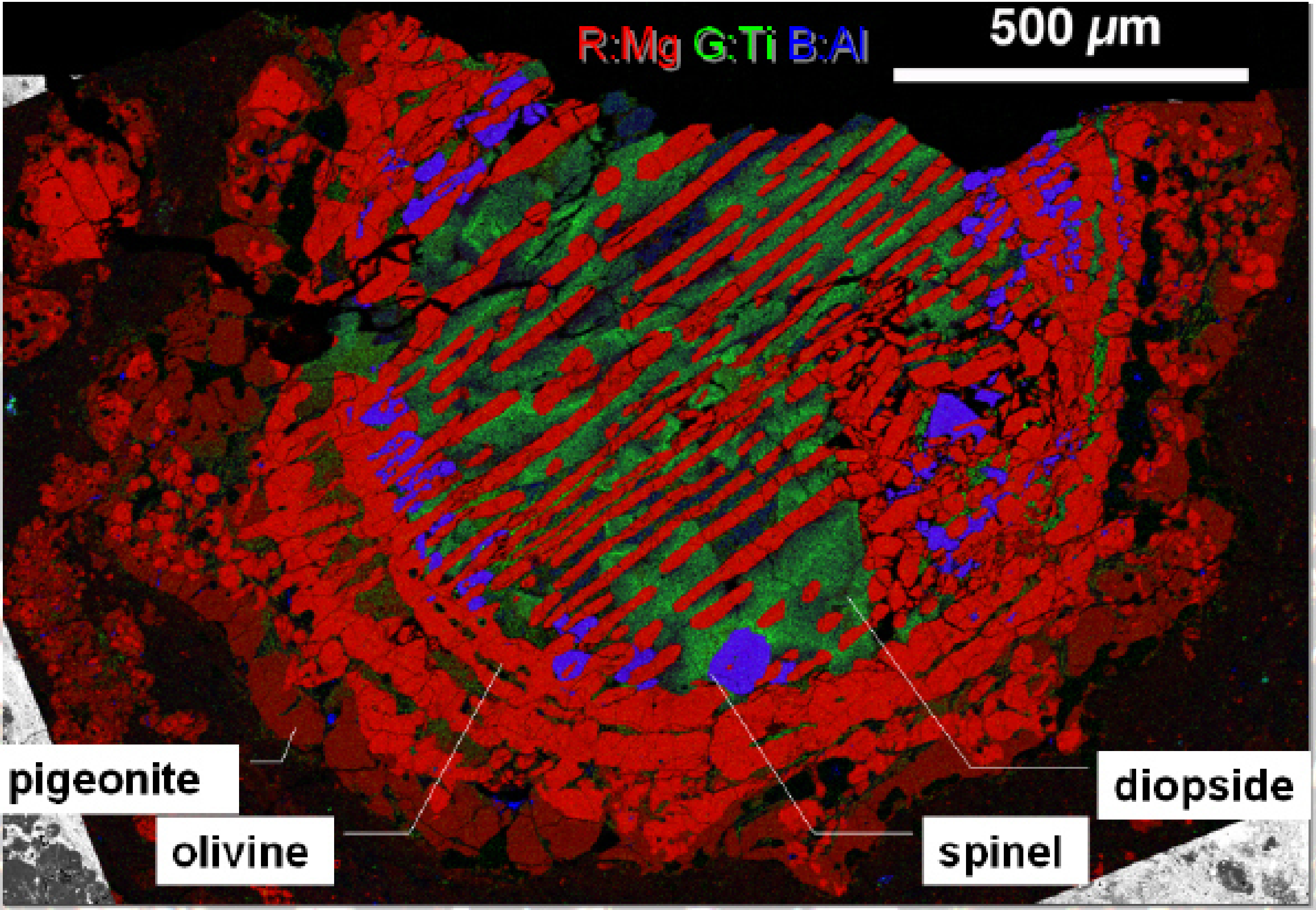

Petrography of C1m (Enveloping compound chondrule)

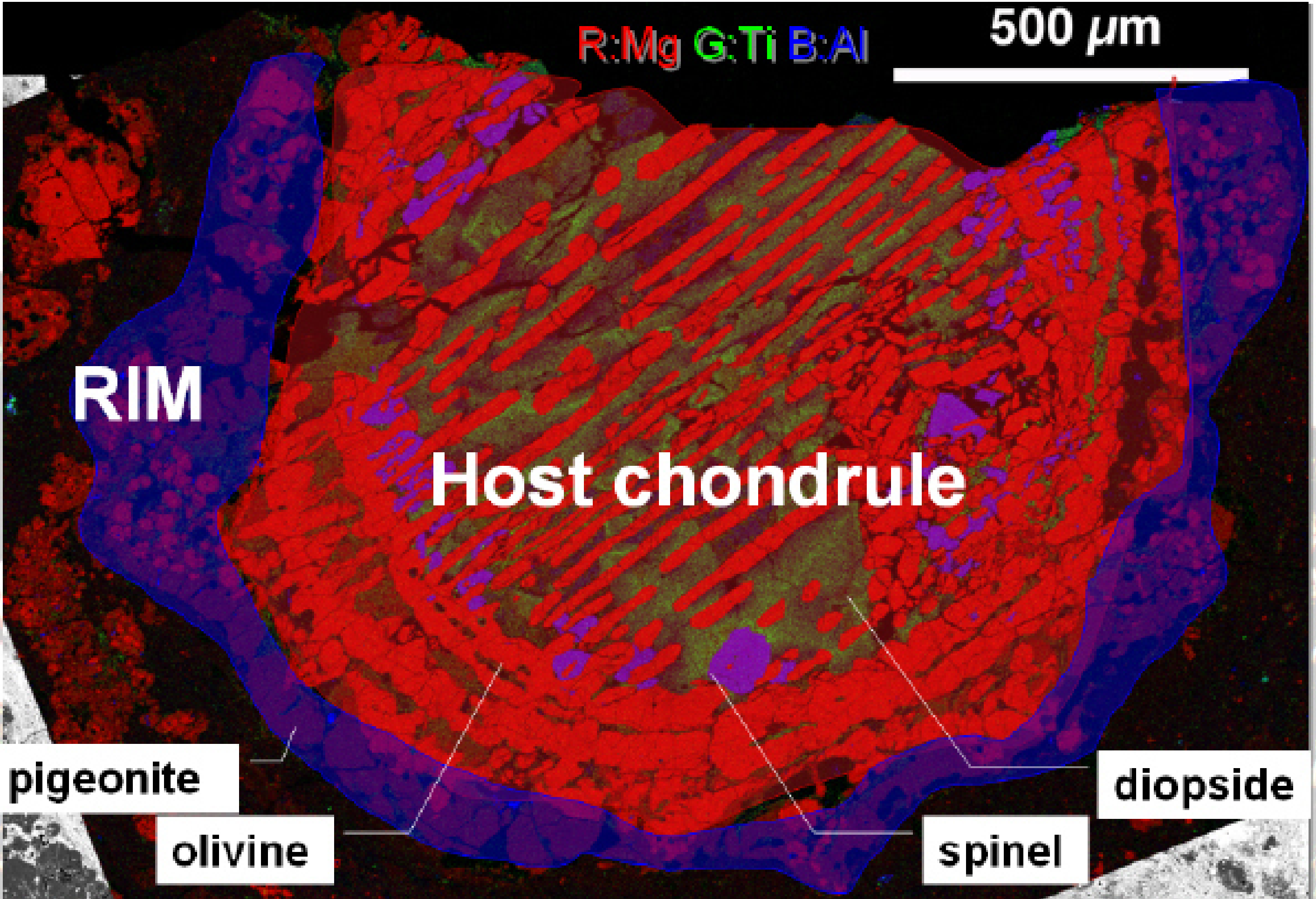

Petrography of C1m (SIMS measurements points)

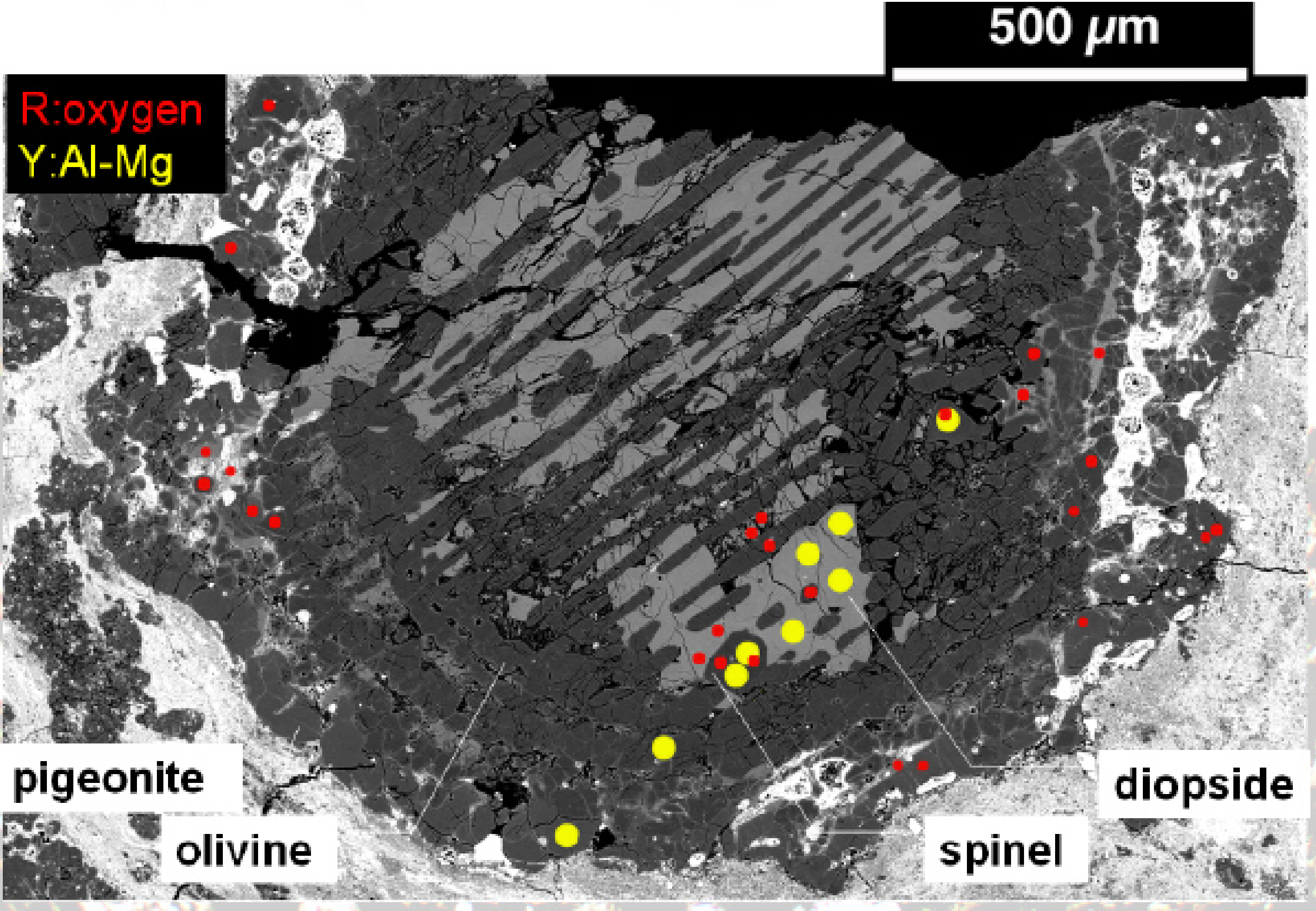

Oxygen isotopic compositions

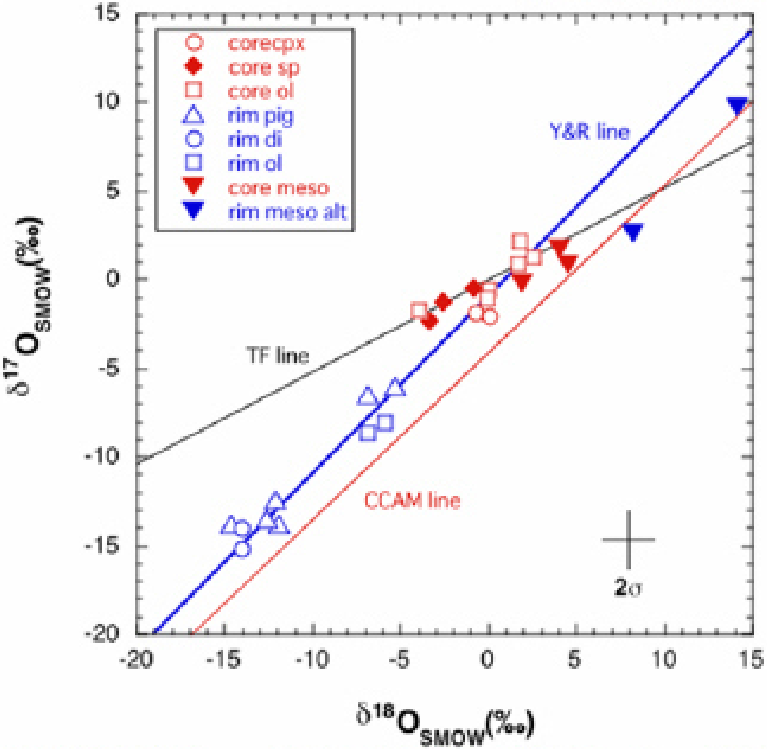

- **Host :**
  - ^{16}O-poor signature

  ($\delta^{17,18}O_{SMOW}$= ~0 ‰)
- **Igneous rim :**
  - ^{16}O-rich relative to that of host

  ($\delta^{17,18}O_{SMOW}$= ~-5 to -15‰)

Oxygen isotopic compositions

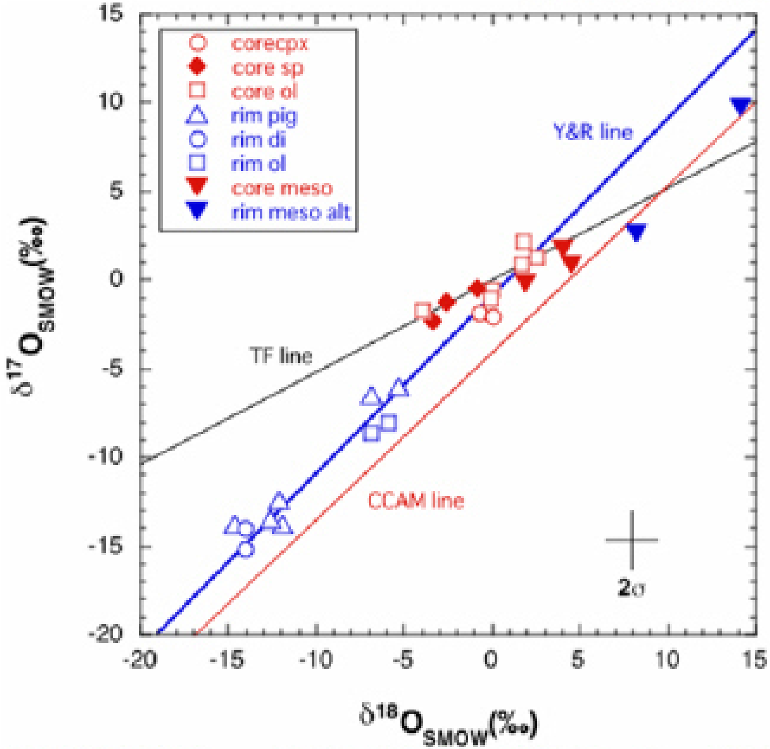

- **Host :**
  - ^{16}O-poor signature

    ($\delta^{17,18}O_{SMOW}$= ~0 ‰)
- **Igneous rim :**
  - ^{16}O-rich relative to that of host

    ($\delta^{17,18}O_{SMOW}$= ~-5 to -15‰)

Oxygen isotope disequilibrium between host and igneous rim.

Al-Mg isotope diagram of C1m

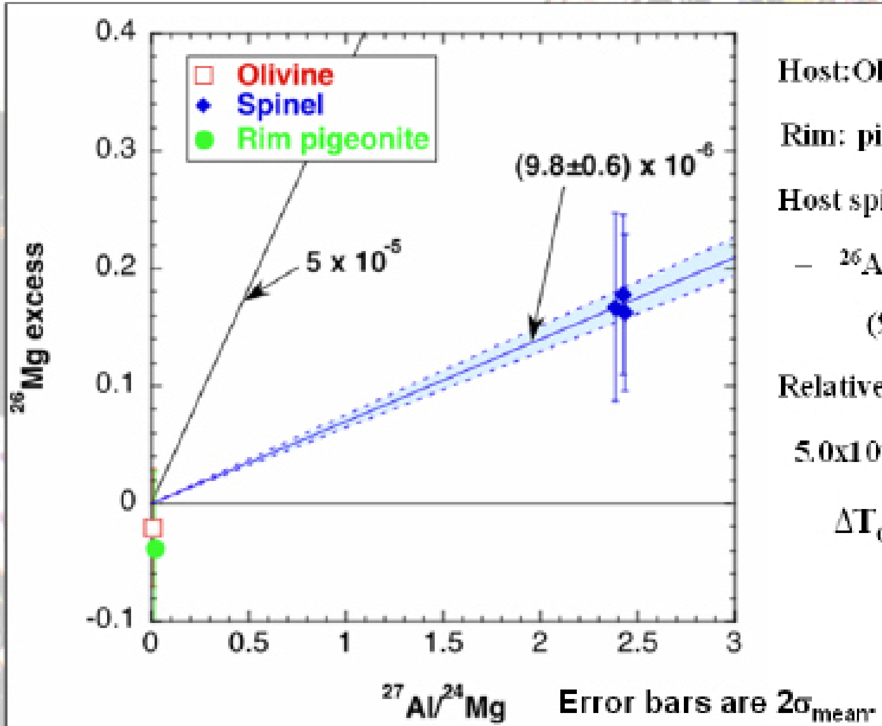

Host:Olivine, spinel

Rim: pigeonite

Host spinel shows clear ^{26}Mg excesses.

– ^{26}Al initial ratio:

$(9.8 \pm 0.6) \times 10^{-6}$

Relative age after CAI formation

$5.0 \times 10^{-5}{}_{CAI} \rightarrow (9.8 \pm 0.6) \times 10^{-5}{}_{C1m}$

$\Delta T_{CAI} = 1.7 \pm 0.1$ Myr

Al-Mg isotope diagram of C1m

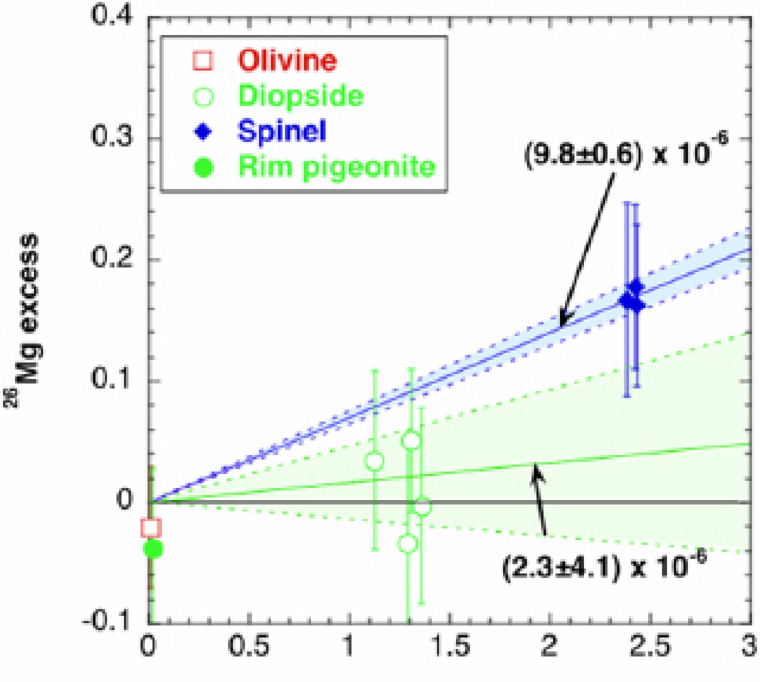

Error bars are $2\sigma_{mean}$.

Diopside

– ^{26}**Al initial ratio:**

$(2.3 \pm 4.1)\times10^{-6}$

$(9.8 \pm 0.6)\times10^{-6}{}_{c1m} \rightarrow (2.3 \pm 4.1)\times10^{-6}{}_{C1m}$

$\Delta T_{chd} = 1.5^{-1.1}_{+6.4}$ Myr

Errors are 2σ.

- **At least 0.4Myr time difference.**

原始太陽系円盤ガスの酸素同位体変動

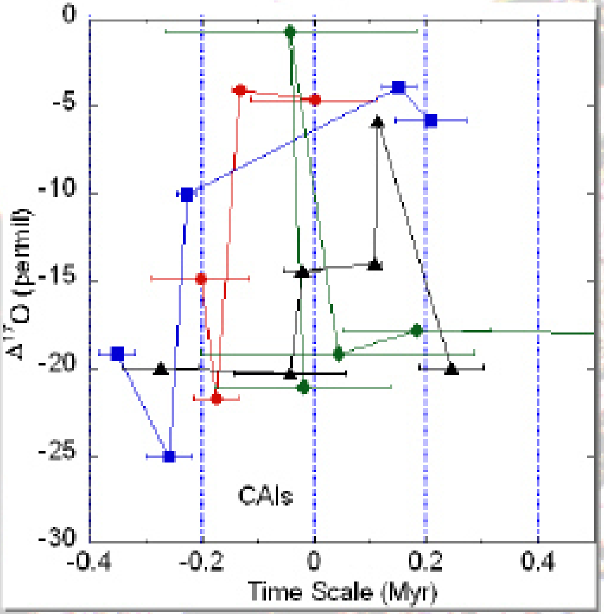

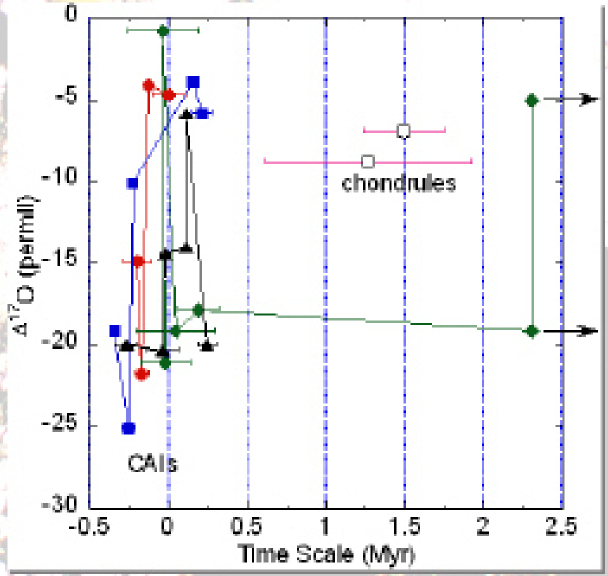

- １個のCAIの形成期間（一瞬〜数百万年）
- １個のCAI周辺の円盤ガスは10万年より短い間に異なる酸素同位体比をもつものに切り替わる。
- 酸素同位体比の切り替わり現象は数百万年間起きている。